

Dynamical collisional energy loss and transport properties of on- and off-shell heavy quarks in vacuum and in the Quark Gluon Plasma

H. Berrehrah,^{1,*} P.B. Gossiaux,^{2,†} J. Aichelin,^{2,‡} W. Cassing,^{3,§} and E. Bratkovskaya^{1,¶}

¹Frankfurt Institute for Advanced Studies and Institute for Theoretical Physics, Johann Wolfgang Goethe Universität, Ruth-Moufang-Strasse 1, 60438 Frankfurt am Main, Germany

²Subatech, UMR 6457, IN2P3/CNRS, Université de Nantes, École des Mines de Nantes, 4 rue Alfred Kastler, 44307 Nantes cedex 3, France

³Institut für Theoretische Physik, Universität Giessen, 35392 Giessen, Germany

In this study we evaluate the dynamical collisional energy loss of heavy quarks, their interaction rate as well as the different transport coefficients (drag and diffusion coefficients, \hat{q} , etc). We calculate these different quantities for i) perturbative partons (on-shell particles in the vacuum with fixed and running coupling) and ii) for dynamical quasi-particles (off-shell particles in the QGP medium at finite temperature T with a running coupling in temperature as described by the dynamical quasi-particles model). We use the perturbative elastic ($q(g)Q \rightarrow q(g)Q$) cross section for the first case, and the Infrared Enhanced Hard Thermal Loop cross sections for the second. The results obtained in this work demonstrate the effects of a finite parton mass and width on the heavy quark transport properties and provide the basic ingredients for an explicit study of the microscopic dynamics of heavy flavors in the QGP - as formed in relativistic heavy-ion collisions - within transport approaches developed previously by the authors.

PACS numbers: 24.10.Jv, 02.70.Ns, 12.38.Mh, 24.85.+p

I. INTRODUCTION

In ultrarelativistic heavy-ion collisions there is strong circumstantial evidence that gluons and light quarks (u, d, s) come to an equilibrium and form a plasma of quarks and gluons (QGP) [1–6]. As a consequence, mesons and baryons containing only light quarks are formed with a multiplicity which corresponds to that expected for a system in statistical equilibrium. This observation limits strongly the use of such mesons and baryons to study the properties of the QGP during its expansion because after thermal freeze out the information about the previous phase is lost. Heavy quarks (c and b) do not come to an equilibrium with the plasma degrees of freedom and may therefore serve as a probe to study the properties of the deconfined system in the early phase of the reaction.

It has been shown in experiments at the Relativistic Heavy Ion Collider (RHIC) and at the CERN Large Hadron Collider (LHC) accelerators that high momentum charm and bottom quarks experience a remarkable quenching in the QGP despite of their large mass. This quenching is reflected in the nuclear modification factor R_{AA} , i.e. the ratio of the transverse momentum spectra of heavy quarks in heavy-ion collisions to that in proton-proton collisions, properly scaled by the number of binary proton-proton collisions in a heavy-ion reaction. Usually, such a quenching is attributed to the energy loss of heavy quarks in the QGP, although alternative explanations are possible. Besides the R_{AA} , the elliptic flow v_2 of heavy quarks has turned out to be an important observable. Initially neither the heavy quarks, produced in hard collisions, nor the constituents of the plasma have sizeable nonzero elliptic flow. In the hydrodynamically expanding plasma the spatial eccentricity of the overlap region of projectile and target is converted into an elliptic flow in momentum space. In turn, heavy quarks may acquire an elliptic flow by interactions with the plasma constituents. It is remarkable that experimentally the elliptic flow of heavy mesons (including c -quark degrees of freedom) equals almost that of light mesons.

These observations have triggered many studies [7–21], first by exploiting the single-electron data [22–26], later by investigating identified D -mesons. Despite of the many efforts a consensus on how to treat the interactions of heavy quarks with the plasma has not been reached yet. Early predictions adopted the natural starting point to calculate the elastic interaction of the heavy quarks with the constituents of the plasma, the light quarks and gluons, on the basis of perturbative QCD (pQCD) scattering cross sections, making a rather arbitrary choice of the coupling constant and the infrared regulator of the gluon propagator. These calculations underestimate significantly the energy loss and the elliptic flow of heavy quarks, i.e. the coupling of heavy quarks with the QGP. Later on radiative energy loss has been considered. It increases the energy loss but it is difficult to calculate due to the interplay between Landau Pomeranchuk Migdal (LPM) effects and the rapid medium expansion. In addition, it has also been suggested that heavy hadronic resonances could be formed in the plasma which might yield an additional energy loss [26].

* berrehrah@fias.uni-frankfurt.de

† gossiaux@subatech.in2p3.fr

‡ aichelin@subatech.in2p3.fr

§ wolfgang.cassing@theo.physik.uni-giessen.de

¶ brat@th.physik.uni-frankfurt.de

To be comparable with the experimental data these elementary interactions between heavy quarks and the plasma constituents have to be embedded in a model which describes the expansion of the QGP itself. The description of this expansion is not unique and different expansion scenarios may easily change the R_{AA} and v_2 values by a factor of two [27]. This observation, as well as the many parameters which enter the calculations of the elementary interaction between heavy quarks and plasma constituents, which include quark and gluon masses, coupling constants, spectral functions and infrared cutoffs, make it useful to study transport coefficients in which the complicated reaction dynamics is reduced to a couple of coefficients which can be directly compared between different models (or with correlators from lattice QCD). It is the purpose of this article to present these transport coefficients for different models in continuation of Ref. [28] in which the different elementary cross sections have been computed.

In line with Ref. [28] we concentrate on the following models:

- HTL-GA (Hard Thermal Loop-Gossiaux Aichelin) approach. The details of this model can be found in Refs. [19, 28, 29]. As compared to former pQCD approaches this model differs in the description of the interaction between the heavy quarks and the plasma particles in two respects:
 - an effective running coupling constant extended in the non-perturbative domain that remains finite at vanishing four-momentum transfer $t \rightarrow 0$ in line with [30].
 - an infrared regulator μ in the t -channel which is determined from hard thermal loop calculations of Braaten and Thoma [31] including a running coupling α . In practice, we use an effective gluon propagator with a 'global' $\mu^2 = \kappa \tilde{m}_D^2$, where $\tilde{m}_D^2(T) = \frac{N_c}{3} \left(1 + \frac{N_f}{6}\right) 4\pi\alpha(-\tilde{m}_D(T)) T^2$, for $qQ \rightarrow qQ$ and $gQ \rightarrow gQ$ scattering. The parameter κ is determined by requiring that the energy loss dE/dx , obtained with this effective propagator, reproduces the running coupling α result in the extended HTL calculation in the t -channel from Refs. [20, 23, 29]. The resulting value is $\kappa \approx 0.2$. The details of this model are described in the appendix of Ref. [19].

Using the latter ingredients the cross section is increased as compared to the former pQCD studies, especially for small momentum transfer [19, 28, 29]. In the HTL-GA approach we will also consider the case of a fixed coupling constant ($\alpha = 0.3$) and of a Debye mass $m_D \approx \xi g_s T$ with $\xi = 1$ as infrared regulator, even if such naive pQCD calculations are unable to reproduce the data, neither the energy loss nor the elliptic flow. The aim is to make contact with the previous calculations where the gluon propagator in the t -channel Born matrix element has to be IR regulated by a fixed screening mass μ [9, 32]. We will also report the results from standard pQCD calculations if available (cf. Moore and Teaney [11]).

In the HTL-GA approach, the heavy quarks are considered massive while the gluons and light quarks are massless. Nevertheless, we will study the effects of finite masses of gluons and light quarks on the transport properties of the heavy quarks, too.

- IEHTL (Infrared Enhanced Hard Thermal Loop) approach: This approach takes into account nonperturbative spectral functions and self-energies of the quarks, antiquarks and gluons in the QGP at finite temperature. For this purpose, we use parametrizations of the quark and gluon masses and coupling constants provided by the dynamical quasi-particle model (DQPM) which are determined to reproduce lattice quantum chromodynamics (lQCD) results [33–40] at finite temperature and vanishing quark chemical potential μ . In this approach, the gluons and light and heavy quarks have finite masses and widths.
- DpQCD (Dressed perturbative QCD) approach: In this approach the spectral functions of the IEHTL approach are replaced by the DQPM pole masses for the incoming, outgoing and exchanged quarks and gluons. In this model the gluons and light and heavy quarks are massive but have zero widths.

The different models presented here aim to describe the heavy meson spectra and are related to the fundamental parameters of the microscopic interactions of heavy quarks with the QGP partons. The mesoscopic quantities, characterizing the transport properties of a heavy quark propagating in the QGP, are the transport coefficients formally expressed by the variable \mathcal{X} . Their time evolution is given for on-shell partons by

$$\frac{d\langle \mathcal{X}^{\text{on}} \rangle}{d\tau} = \sum_{q,g} \frac{1}{(2\pi)^5 2M_Q} \int \frac{d^3 q}{2E_q} f(q) \int \frac{d^3 q'}{2E_{q'}} \int \frac{d^3 p'}{2E_{p'}} \delta^{(4)}(P_{in} - P_{fin}) \mathcal{X} \frac{1}{g_Q g_p} \sum_{k,l} |\mathcal{M}_{2,2}^{\text{on}}(p, q; i, j | p', q'; k, l)|^2. \quad (\text{I.1})$$

Here the indices (i, j) stand for the discrete quantum numbers (spin s , flavor f and color c) of the initial heavy quark (with the momentum p , mass M_Q , energy $E_p = \sqrt{\mathbf{p}^2 + M_Q^2}$ and velocity v_Q) and the initial light quark or gluon (with the momentum q , mass m_q , energy $E_q = \sqrt{\mathbf{q}^2 + m_q^2}$ and velocity v_q) while (k, l) denote those of the heavy quark (with the momentum p') and

of the light quark/gluon (with the momentum q') in the final state. g_Q is the degeneracy factor of the heavy quark ($g_Q = 6$) and g_p is the degeneracy factor of the parton ($g_p = 6$ for light quarks, $g_p = 16$ for massless gluons and $g_p = 24$ for massive gluons). Furthermore, $\sum_{q,g}$ denotes the sum over the light quarks and gluons of the medium while $|\mathcal{M}_{2,2}(p, q; i, j|p', q'; k, l)|^2$ is the transition matrix-element squared, related to the cross section $\sigma_{2 \rightarrow 2}$ by:

$$\frac{1}{(2\pi)^6} \int \frac{d^3 q'}{2E_{q'}} \frac{d^3 p'}{2E_{p'}} (2\pi)^4 \delta^{(4)}(P_{in} - P_{fin}) \frac{1}{g_Q g_p} \sum_{k,l} |\mathcal{M}_{2,2}(p, q; i, j|p', q'; k, l)|^2 = 2\lambda(s, m_q^2, M_Q^2) \sigma_{2 \rightarrow 2}(\sqrt{s}), \quad (I.2)$$

with

$$2\lambda(s, m_q^2, M_Q^2) = 4E_p E_q |v_Q - v_q| \quad (I.3)$$

denoting the flux of the incoming particles and $\lambda(a, b, c) = a^2 + b^2 + c^2 - 2ab - 2ac - 2bc$.

Depending on the choice of \mathcal{X} one can address different transport coefficients: For $\mathcal{X} = 1$, $\mathcal{X} = (E - E')$, $\mathcal{X} = (\mathbf{p} - \mathbf{p}')$, $\mathcal{X} = (p - p')^\mu (p - p')^\nu$, the formula (I.1) corresponds, respectively, to the interaction rate $\mathcal{R}(p, T) = \frac{dN_{coll}}{d\tau}$, the energy loss $\frac{dE}{d\tau}(p, T)$, the drag coefficient $\mathcal{A}(p, T)$ and finally the diffusion coefficient $\mathcal{B}^{\mu\nu}(p, T)$, all evaluated per unit proper time τ in the rest system of the heavy quark.

In our study we use (I.1) for the case of on-shell heavy quarks and partons with the transition amplitudes $\sum |\mathcal{M}_{2,2}|^2 \equiv \sum |\mathcal{M}_{2,2}^{HTL-GA}|^2$, $\sum |\mathcal{M}_{2,2}^{DpQCD}|^2$. Replacing the on-shell phase-space measure in (I.1) by the off-shell equivalent

$$\begin{aligned} Tr_{(i)}^{on} &= \int \frac{d^3 p_i}{(2\pi)^3 2E_i} \rightarrow Tr_{(i)}^{off} = \int \frac{d^4 p_i}{(2\pi)^4} \rho_i(p_i) \Theta(\omega_i), \\ \frac{1}{2E_p} &\rightarrow \int \frac{d\omega}{2\pi} \rho_p(\omega) \theta(\omega), \end{aligned} \quad (I.4)$$

where ρ_i is the spectral function of the off-shell particle i and Θ denotes the Heaviside function, one can extend (I.1) to the case of off-shell partons to

$$\frac{d\langle \mathcal{X}^{off} \rangle}{d\tau} = \sum_{q,g} \frac{1}{(2\pi)^9} Tr_q^{off} Tr_p^{off} Tr_{q'}^{off} Tr_{p'}^{off} f(\mathbf{q}) \delta^{(4)}(P_{in} - P_{fin}) \mathcal{X} \frac{1}{g_Q g_p} \sum_{k,l} |\mathcal{M}_{2,2}^{off}(p, q; i, j|p', q'; k, l)|^2, \quad (I.5)$$

with $\sum |\mathcal{M}_{2,2}^{off}|^2 \equiv \sum |\mathcal{M}_{2,2}^{IEHTL}|^2$ as explained above.

In this study we will address the different transport coefficients of a heavy quark in a static medium at finite temperature. They give the response of the medium to the propagation of a heavy quark under fixed thermodynamical conditions. For out-of-equilibrium microscopic dynamics of the heavy quarks in the QGP, a description of the medium evolution is required. This study is beyond the scope of this paper and can be realized within the Parton-Hadron-String-Dynamics (PHSD) or Monte-Carlo α_s Heavy Quarks (MC@HQ) transport approaches.

The paper is organized as follows: In Sec. II we first briefly recall the Dynamical Quasi-Particle Model in order to fix the main ingredients used in the DpQCD/IEHTL approaches. In Section III we evaluate the elastic interaction rate and the relaxation time for the approaches introduced above. The calculation of the transport coefficients is performed on the basis of these cross sections. In Sections IV and V we calculate the drag coefficient as well as the energy loss per unit length and the spatial diffusion coefficient. Both the drag and diffusion coefficients are the transport coefficients which are necessary for Fokker-Planck transport approaches describing the time evolution of the heavy-quark momentum distribution. In Section VI we discuss the transport coefficient \hat{q} , the average change of the square of the transverse momentum per unit length which is strongly related to the transverse diffusion. Finally, in Section VII we evaluate the transport cross section and perform a critical analysis of the applicability of the independent collision approach. We conclude in Section VIII with a summary of our findings.

II. REMINDER OF THE DYNAMICAL QUASI-PARTICLE MODEL

The dynamical quasi-particle model [34, 35, 37] describes QCD properties in terms of “resummed” single-particle Green’s functions (in the sense of a two-particle irreducible (2PI) approach) and leads to a quasi-particle equation of state, which reproduces the QCD equation of state extracted from lattice QCD calculations in Ref. [41, 42]. According to the DQPM, the constituents of the strongly coupled Quark Gluon Plasma (sQGP) are strongly interacting massive partonic quasi-particles. Details of the approach can be found in [28]. Due to the finite imaginary parts of the selfenergies the partons of type “ i ” are described by spectral functions $\rho_i(p)$ for which we can assume one of the following forms:

i) Lorentzian- ω form: the spectral function $\rho_i(p)$, with $p = (\omega, \mathbf{p})$, is given by [36–40]

$$\rho_i^L(\omega) = \frac{\gamma_i}{\tilde{E}_i} \left(\frac{1}{(\omega - \tilde{E}_i)^2 + \gamma_i^2} - \frac{1}{(\omega + \tilde{E}_i)^2 + \gamma_i^2} \right) \equiv \frac{4\omega\gamma_i}{(\omega^2 - \mathbf{p}^2 - M_i^2)^2 + 4\gamma_i^2\omega^2}.$$

with: $\tilde{E}_i^2(\mathbf{p}) = \mathbf{p}^2 + M_i^2 - \gamma_i^2$, and $i \in [g, q, \bar{q}, Q, \bar{Q}]$. (II.1)

This spectral function (II.1) is antisymmetric in ω and normalized as

$$\int_{-\infty}^{+\infty} \frac{d\omega}{2\pi} \omega \rho_i^L(\omega, \mathbf{p}) = \int_0^{+\infty} \frac{d\omega}{2\pi} 2\omega \rho_i^L(\omega, \mathbf{p}) = 1. \quad (II.2)$$

M_i, γ_i are the particle pole mass and width, respectively.

ii) Breit-Wigner- m form: the spectral function $\rho_i(p)$ is given by the Breit-Wigner distribution:

$$\rho_i^{BW}(m_i) = \frac{2}{\pi} \frac{m_i^2 \gamma_i^*}{(m_i^2 - M_i^2)^2 + (m_i \gamma_i^*)^2}, \quad \text{with: } \int_0^\infty dm_i \rho_i^{BW}(m_i, T) = 1, \quad (II.3)$$

where M_i is the dynamical quasi-particle (DQPM) mass (i.e pole mass). Here $m \equiv m_i$ is the independent variable; it's related to ω by $\omega^2 = m^2 + \mathbf{p}^2$ while γ^* is related to γ by the relation $2\omega\gamma = m\gamma^*$.

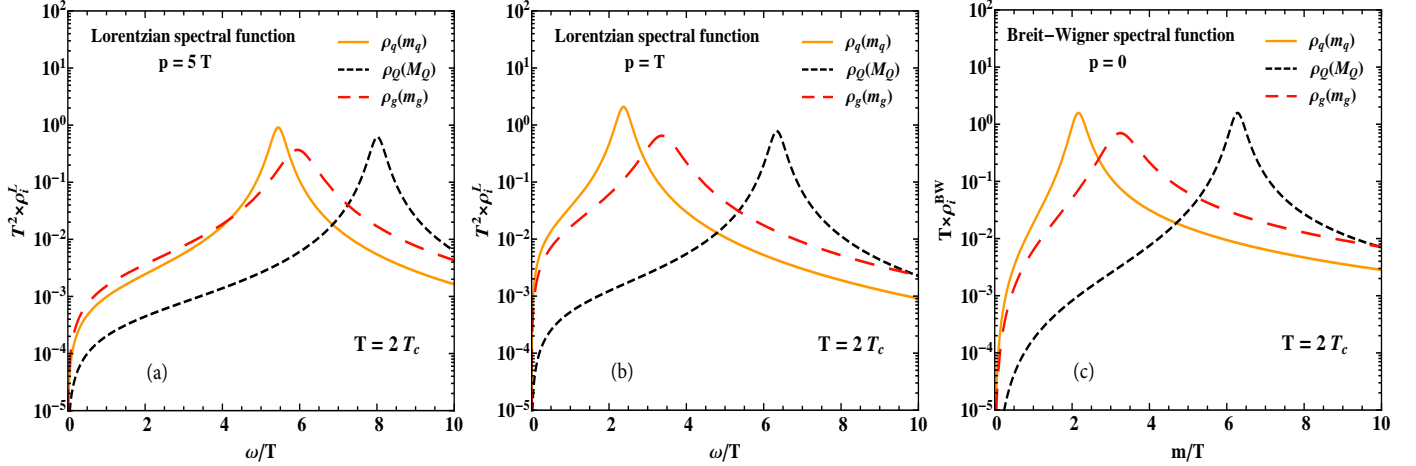


FIG. 1. (Color online) The DQPM spectral functions of light quarks, heavy quarks and gluons of (II.1)-(II.3) for $T/T_c = 2$ ($T_c = 0.158$ GeV). γ_i and M_i can be found in [28]. Left (a) (Center (b)): The Lorentzian spectral function as a function of ω/T for $p = 5 T$ ($p = T$). Right (c): The Breit-Wigner spectral function as a function of m/T for $p = 0$.

The Breit-Wigner- m form of the spectral function is a non-relativistic approximation of the Lorentzian- ω form (neglecting $\|\mathbf{p}\|$ compared to m , $m \gg \|\mathbf{p}\|$). Figure 1 (l.h.s and center) shows the Lorentzian- ω form as a function of ω/T for different values of the momentum p (the Breit-Wigner- m form as a function of m/T) of the spectral function of gluons, light and heavy quarks for $T = 2T_c$ (r.h.s). One sees that the peaks and the widths of these distributions are different. The Lorentzian- ω shape depends on the momentum $\|\mathbf{p}\|$, whereas the Breit-Wigner- m form is independent of $\|\mathbf{p}\|$. Comparing the figures 1-left and center, we notice that an increasing momentum leads to a shift of poles masses to larger values of ω/T .

The pole masses and widths for light quarks and gluons used in the DQPM are displayed in Fig. 2-(a) as a function of T/T_c . The functional forms for the dynamical pole masses of quasiparticles (gluons and quarks) are chosen in a way that they become identical to the perturbative thermal masses in the asymptotic high-temperature regime [37–40]. Fig. 2-(a) gives also the light quark and gluon masses in HTL, where $m_q = m_g/\sqrt{3}$ and $m_g = \tilde{m}_D(T)/\sqrt{3}$, with $\tilde{m}_D^2(T) = \frac{N_c}{3} \left(1 + \frac{N_f}{6} \right) 4\pi\alpha(-\tilde{m}_D(T)) T^2$.

Figure 2-(b) shows the infrared regulator μ^2 used in the t-channel as a function of the medium temperature following the different models presented in the introduction. We recall that μ^2 is identical to the DQPM gluon mass squared in the DpQCD model and is given by $\mu^2 = \frac{N_c}{3} \left(1 + \frac{N_f}{6}\right) 4\pi\alpha T^2$ for the model HTL-GA with constant α and by $\mu^2 = \kappa \tilde{m}_D^2$, where $\kappa \approx 0.2$ for the HTL-GA model with running α . The small value of μ^2 observed in HTL-GA with α running as compared to the DpQCD value will have a strong effect on the transport coefficients (see below).

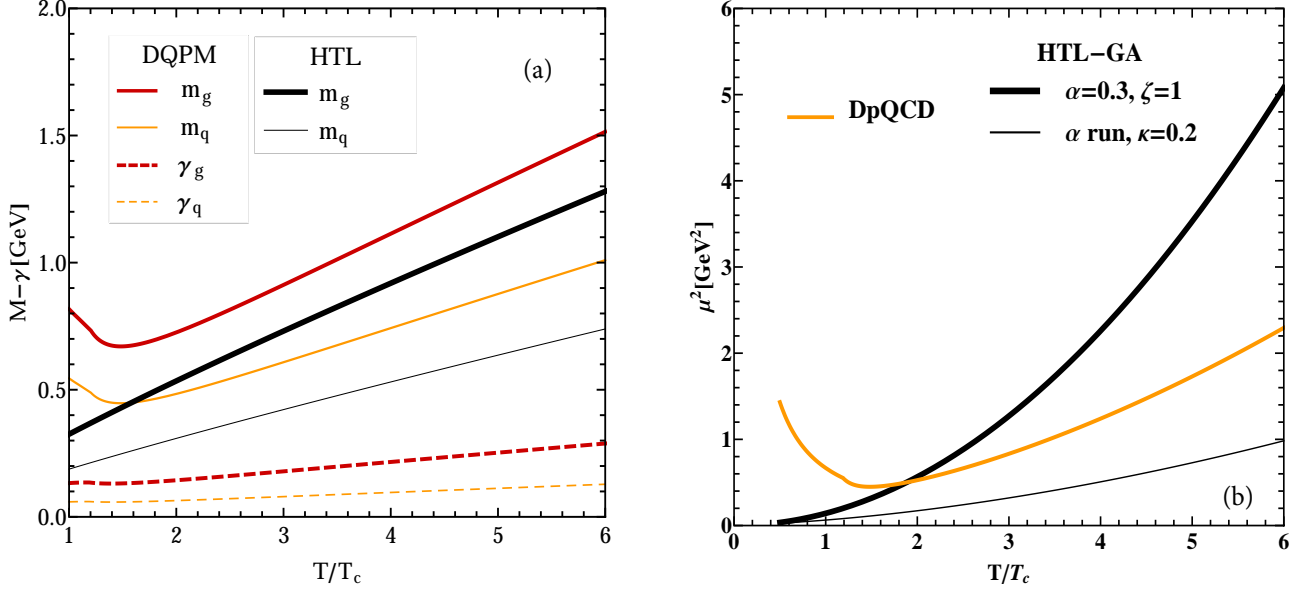


FIG. 2. (Color online) Masses and widths of light quarks and gluons in the DQPM [43] and masses in the HTL as a function of T/T_c ($T_c = 0.158$ GeV) (left). The infrared regulator μ^2 as a function of the temperature T/T_c given in HTL-GA as well as in the DpQCD model (right). The parameters ξ , κ and α in the HTL-GA model are described in the introduction.

III. ELASTIC INTERACTION RATE AND THE ASSOCIATED RELAXATION TIME

We start out with the elastic interaction rate, i.e. the rate of the interaction of a heavy quark with momentum \mathbf{p} propagating through a QGP in thermal equilibrium at a given temperature T . The quarks of the plasma are described by a Fermi-Dirac distribution $f_q(\mathbf{q}) = \frac{1}{e^{E_q/T} + 1}$ whereas the gluons follow a Bose-Einstein distribution $f_g(\mathbf{q}) = \frac{1}{e^{E_g/T} - 1}$. Therefore, the interaction rates are temperature dependent. In our calculation we use the elastic scattering cross sections of Ref. [28] for $q(\bar{q})Q$ and gQ collisions, for on-shell as well as for off-shell partons.

A. Elastic interaction rates for on-shell partons

For on-shell particles (and in the reference system in which the heavy quark has the velocity $\boldsymbol{\beta} = \mathbf{p}/E_p$) the interaction rate for $2 \rightarrow 2$ collisions is given by $R^{\text{on}}(\mathbf{p}) = \frac{dN_{\text{coll}}^{2 \rightarrow 2}}{dt} = \frac{M_Q}{E_p} \frac{dN_{\text{coll}}^{2 \rightarrow 2}}{d\tau}$ (see eq.(I.1)). We introduce the invariant quantity

$$\begin{aligned}
 r^{\text{on}}(s) &= \frac{1}{(2\pi)^2} \int \frac{d^3 q'}{2E_{q'}} \int \frac{d^3 p'}{2E_{p'}} \delta^{(4)}(P_{\text{in}} - P_{\text{fin}}) \times \frac{1}{g_Q g_p} \sum_{k,l} |\mathcal{M}_{2,2}(p, q; i, j | p', q'; k, l)|^2 \\
 &= \frac{p_{cm}}{16\pi^2 \sqrt{s}} \int d\Omega_{q'} \frac{1}{g_Q g_p} \sum_{k,l} |\mathcal{M}_{2,2}(p, q; i, j | p', q'; k, l)|^2(s, \Omega_{q'}) \\
 &= \frac{\pi}{16\pi^2 \sqrt{s}} \frac{1}{p_{cm}(s)} \int_{-4p_{cm}^2}^0 dt \frac{1}{g_Q g_p} \sum_{k,l} |\mathcal{M}_{2,2}(p, q; i, j | p', q'; k, l)|^2(s, t),
 \end{aligned} \tag{III.1}$$

where

$$p_{cm} = \lambda^{1/2}(s, m_q^2, M_Q^2)/(2\sqrt{s}), \quad (\text{III.2})$$

is the momentum of the scattering partners in the c.m. frame. The interaction rate in the plasma rest system for a heavy quark with momentum \mathbf{p} is given, following (I.1), by

$$R^{\text{on}}(\mathbf{p}) = \sum_{q,g} \frac{1}{2E_p} \int \frac{d^3q}{(2\pi)^3} \frac{1}{2E_q} f(\mathbf{q}) r^{\text{on}}(s) = \sum_{q,g} \int \frac{d^3q}{(2\pi)^3} f(\mathbf{q}) |v_Q - v_q| \sigma(s), \quad (\text{III.3})$$

where $\sum_{q,g}$ denotes the sum over the light quarks and gluons of the medium. The integral in the middle of (III.3) does not depend on the reference frame and therefore it is convenient to perform the calculation in the rest frame of the heavy quark,

$$R^{\text{on}}(\mathbf{p} = 0) = \sum_{q,g} \frac{1}{2M_Q} \int \frac{d^3q}{(2\pi)^3} \frac{1}{2E_q} f_r(\mathbf{q}) r^{\text{on}}(s), \quad (\text{III.4})$$

where $f_r(\mathbf{q})$ is the invariant distribution of the plasma constituents in the rest frame of the heavy quark:

$$\int d\Omega f_r(\mathbf{q}) = 2\pi \int d\cos\theta \frac{1}{e^{(u^0 E_q - \mathbf{u} \cdot \mathbf{q} \cos\theta)/T} \pm 1}, \quad (\text{III.5})$$

with $u \equiv (u^0, \mathbf{u}) = \frac{1}{M_Q}(E_p, -\mathbf{p})$ being the fluid 4-velocity measured in the heavy quark rest frame, while θ is the angle between \mathbf{q} and \mathbf{u} .

B. Elastic interaction rates for off-shell partons

For off-shell partons the elastic interaction rate (I.5) is obtained by replacing $\int \frac{d^3p}{(2\pi)^3} \frac{1}{2E_p}$ by $\int \frac{d^4p}{(2\pi)^4} \rho(p) \Theta(p_0)$ with $\rho(p)$ being the spectral function which can be specific for each particle species (I.4). For the two forms of spectral functions, the Lorentzian- ω form and the Breit-Wigner- m form, the explicit results are given in appendix A for completeness.

The total interaction rate of the off-shell approach (IEHTL) in the plasma rest system is compared to that of the on-shell calculations (HTL-GA and DpQCD) (III.3) in figure 3-(a) and (b) as a function of the momentum of the heavy quark, p_Q and the temperature, respectively. We assume here a Breit-Wigner spectral function and a Boltzmann-Jüttner distribution for both, the light quarks and the gluons. Our results are rather independent of the choice of the spectral function and of whether the Boltzmann-Jüttner distribution is replaced by a Fermi/Bose distribution. In figures 3-(a) and (b), the thick black line refers to the case where a constant α and a Debye mass $m_D = \xi g_s T$ with $\xi = 1$ as infrared regulator μ are used, whereas the thin black line gives the result for a constant running coupling and $\mu^2 = \kappa \tilde{m}_D^2$, with $\tilde{m}_D^2(T) = \frac{N_c}{3} \left(1 + \frac{N_f}{6}\right) 4\pi\alpha(-\tilde{m}_D(T^2)) T^2$ and $\kappa = 0.2$ in HTL-GA model. If we give a finite mass to the light quark and gluon ($m_{q,g} = m_{q,g}^{\text{HTL}}$) as shown in figure 2-a) in the HTL-GA model the total rate changes only moderately as can be seen from the black dotted dashed line. The yellow dashed and red solid lines in figure 3-(a) and (b) display the results for the DpQCD and IEHTL models, respectively. As expected, the rates decrease when $m_{q,g}$ increases because the number of plasma collision particles becomes smaller. The reduction factor due to a finite mass is almost independent of $p_Q \geq M_Q$ and therefore the ratio $\text{Rate}(\text{massive } q, g)/\text{Rate}(\text{massless } q, g)$ in the HTL-GA model shows only a weak temperature dependence.

A running coupling with an effective Debye mass of $\kappa \tilde{m}_D$ yields a larger cross section than a fixed coupling constant $\alpha = 0.3$. Naturally this increases the interaction rate if the mass of the particles does not change. Even in regions where the masses of gluons and quarks in the HTL-GA model are not very different from those in the DpQCD approach (cf. Fig.2-a) the rates differ significantly. Therefore, the finite mass of light quark and gluons explains only part of the much lower interaction rate observed for the former model. The remaining difference is due to the cross sections which are lower in the DpQCD approach as compared to HTL-GA, Ref.[28].

The description of the interaction between the heavy quark and the partons of the medium differs between the models. Whereas the coupling constant is strong in the HTL-GA (with α running) and DpQCD/IEHTL models, the coupling is weak in HTL-GA for constant coupling α . On the other hand the interaction has a large range in HTL-GA (with α running) due to a small infrared regulator and it has an intermediate range in the DpQCD/IEHTL and HTL-GA for constant coupling α .

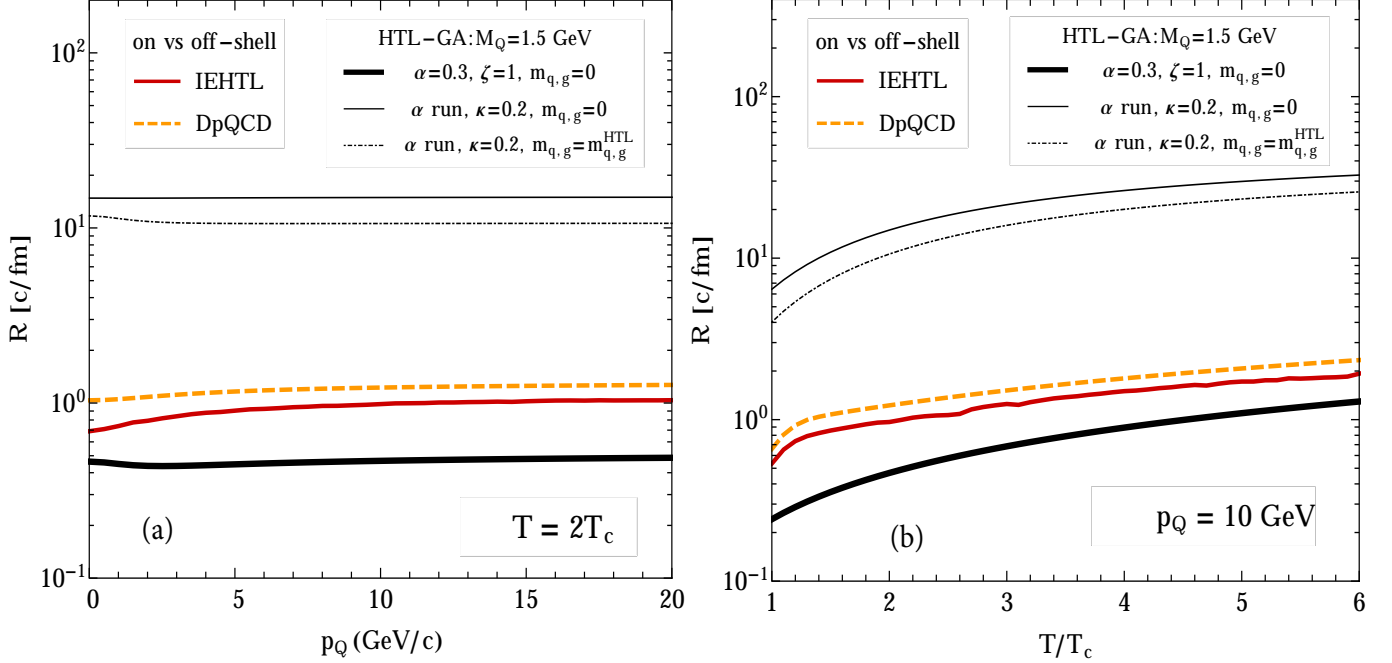


FIG. 3. (Color online) R , the total elastic interaction rate of c -quarks in the plasma rest frame for the three different approaches as a function of the heavy quark momentum for $T = 2T_c$ ($T_c = 0.158$ GeV) (left) and as a function of the temperature T for a heavy quark momentum $p_Q = 10$ GeV (right). The parameters ξ , κ and α in the HTL-GA model are described in the introduction.

We see from Figs. 3-(a) and (b) that the spectral function decreases the interaction rate of heavy quarks with the medium on the order of 20%. This modification is rather independent of the heavy quark momentum and of the temperature of the plasma.

The difference between the DpQCD and IEHTL rates is related on one side to the propagator, which contains an additional imaginary part proportional to the gluon width in the IEHTL model, and on the other side to the asymmetry of the Breit-Wigner spectral function. For finite $\gamma_{g,q,Q}$ width, the contribution of larger masses in the Breit-Wigner spectral function (right side of the pole mass) is larger compared to smaller masses (left side of the pole mass), i.e. with broader gluon and light/heavy quark in the mass distribution, the average mass is shifted to higher values of $m_{g,q,Q}$. This implies that the heavy quark is getting more massive on average and consequently is slowing down in momentum/velocity. Therefore, the number of interactions/per unit length becomes smaller, as shown in figure 3-(a) and (b).

The HTL-GA approach (with running coupling) and massless light quarks and gluons gives by far the largest rate. Besides having the largest cross section [28], the massless nature of the QGP constituent increase the number of possible elastic interactions. Even a finite mass lowers the rate not substantially.

The dependence of the rates on the medium temperature T for an intermediate heavy quark momentum ($p_Q = 10$ GeV) is illustrated in figure 3-(b). All models show an increase of the interaction rate with temperature. The linear dependence seen for the HTL-GA model with $\alpha = 0.3$ and $\xi = 1$ can be easily explained since $R \propto n \times \sigma \propto T$, where $n \propto T^3$ is the parton density and $\sigma \propto T^{-2}$ is the total cross section in this model. As studied in Ref. [28] the temperature dependence of the total cross section differs from one model to another due to the different coupling constants and infrared regulators employed. The extra decrease of the rate in the DPQCD/IEHTL models for small temperature is related to the temperature dependence of the DQPM parton masses (cf. Fig.2-a).

The number of heavy quark elastic collisions per Fermi at $T = 2T_c$ and for an intermediate heavy quark momentum ($p_Q = 10$) is 18.4 for HTL-GA (running coupling constant and $m_q = m_g = 0$) model, 1.37 for DpQCD and 1.06 for IEHTL. These numbers are larger at $T = 5T_c$ with 29.84 elastic collisions per Fermi in the HTL-GA model, 2.07 for DpQCD and 1.72 for IEHTL.

C. Relaxation time for on- and off-shell partons

For the transport coefficients one needs to specify the relaxation time τ which can be deduced from the elastic interaction rate $R(T)$ by averaging over the initial heavy-quark momentum. The relaxation time τ is given for the on- and off-shell partons by

$$\begin{aligned}
(\tau_c^{-1})^{\text{on}} &= \frac{1}{n_Q^{\text{on}}} \sum_{j \in q, \bar{q}, g} g_Q \int \frac{d^3 p_Q}{(2\pi)^3} f_Q(p_Q, M_Q, T) R_{jc}^{\text{on}}(p_Q, M_Q^i, m_j^i, M_Q^f, m_j^f). \\
(\tau_c^{-1})^{\text{off}} &= \frac{1}{n_Q^{\text{off}}} \sum_{j \in q, \bar{q}, g} g_Q \iint \frac{d^3 p_Q}{(2\pi)^3} \rho_j(m_j^{i,f}) \rho_j(M_Q^{i,f}) dm_j^{i,f} dM_Q^{i,f} f_Q(p_Q, M_Q, T) R_{jc}^{\text{on}}(p_Q, M_Q^i, m_j^i, M_Q^f, m_j^f), \quad (\text{III.6})
\end{aligned}$$

with $\rho_q(m_q^{i,f})$ and $\rho_Q(M_Q^{i,f})$ being the Breit-Wigner- m spectral functions [28] for the incoming and outgoing light and heavy quark. Furthermore, g_Q is the heavy quark degeneracy factor while $f_Q(p_Q, M_Q, T)$ is the Fermi-Dirac distribution and n_Q the heavy quark density given for the on-shell case n_Q^{on} and the off-shell case n_Q^{off} by

$$\begin{aligned}
n_Q^{\text{on}}(M_Q, T) &= g_Q \int \frac{d^3 p_Q}{(2\pi)^3} f_Q(p_Q; M_Q, T) \\
n_Q^{\text{off}}(T) &= g_Q \iint \frac{d^3 p}{(2\pi)^3} \rho_Q(M_Q) dM_Q f_Q(p_Q; T, m_Q). \quad (\text{III.7})
\end{aligned}$$

The in-medium elastic cross section for qQ , $\bar{q}Q$ and gQ scattering processes have been studied in detail in Ref. [28]. The processes involving chemical equilibration ($Q\bar{Q} \rightarrow g$, $Q\bar{Q} \rightarrow gg$ and $Q\bar{Q} \rightarrow q\bar{q}$) will not be included in the computation of the relaxation time for heavy quarks since their contribution is negligible due to the small probability that 2 of the few heavy quarks interact.

The results for the relaxation time τ_c of charm quarks are shown in figure 4-(a) for the on-shell and off-shell cases at finite temperature T and at $\mu = 0$ in a medium composed by light quarks/antiquarks and gluons. We display the results for the DpQCD/IEHTL and HTL-GA models. From Fig. 4-(a) one deduces that the heavy quark relaxation time is about the same for DpQCD/IEHTL and HTL-GA with fixed coupling. A much shorter relaxation time is seen for HTL-GA with a running coupling.

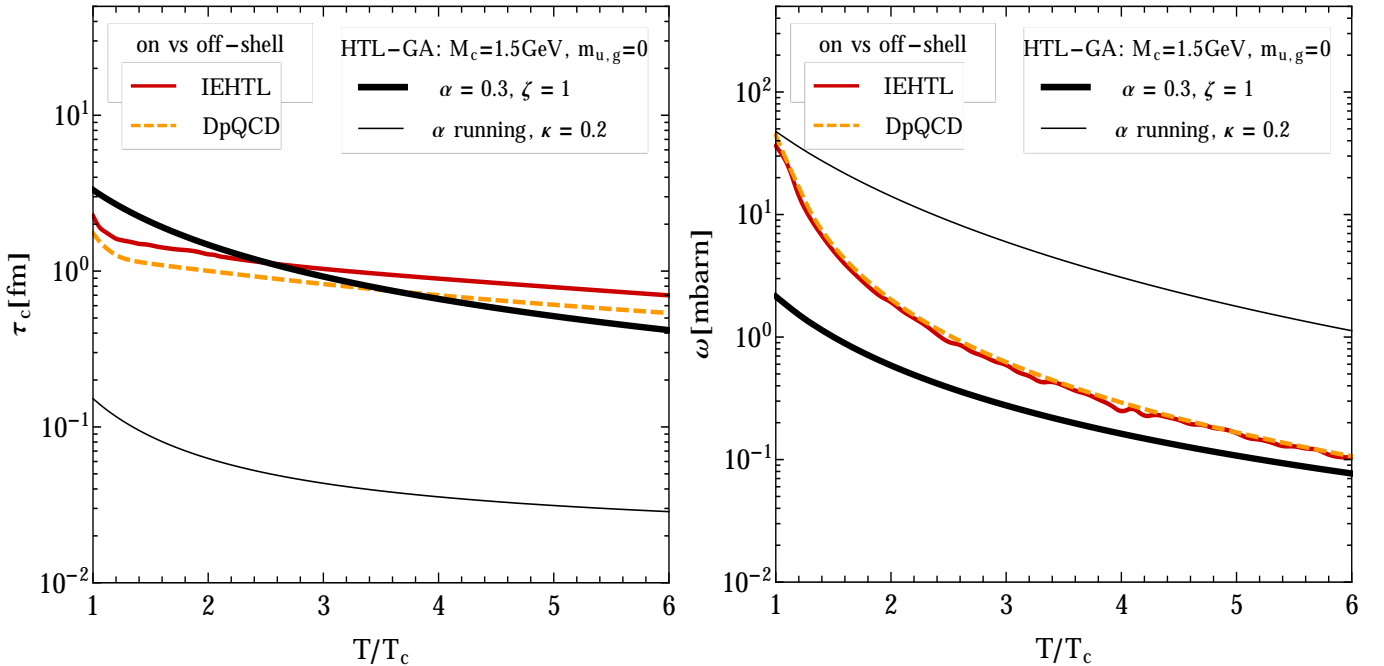


FIG. 4. (Color online) The relaxation time τ_c (left) and the total transition rate $\omega(T)$ (right) for different models as a function of T/T_c with $T_c = 0.158$ GeV at $\mu = 0$ for off-shell (IEHTL, red solid line) and on-shell (DpQCD, yellow dashed line) partons. We consider the DQPM pole masses for the on-shell partons in the DpQCD model and the DQPM spectral functions for the off-shell IEHTL approach. Also shown is a comparison with results in the HTL-GA approaches with constant and running coupling.

Figure 4-(a) shows also that τ_c decreases with temperature since the quark and gluon densities are increasing functions of the temperature. We can evaluate -in terms of powers of T - the behavior of this relaxation time for the different approaches. The density is proportional to T^3 for large temperatures in case of $m \ll T$. The transition rate then is proportional to a power law in

T , i.e. $\sim T^{-\beta}$ with $\beta^{T < 1.2T_c} \sim 2$, $\beta^{T > 1.2T_c} \sim 1.7$ for the HTL-GA model and $\beta^{T < 1.2T_c} \sim 4$, $\beta^{T > 1.2T_c} \sim 2$ for the DpQCD/IEHTL models. Hence, the relaxation time $\tau_c^{T < 1.2T_c} \propto T$ and $\tau_c^{T > 1.2T_c} \propto T^{-1}$ for the DpQCD/IEHTL models. The large exponent in the relaxation times for $T < 1.2 T_c$ in the DpQCD/IEHTL models can be traced back to the infrared enhancement of the effective coupling.

With the established results for the relaxation time we can now calculate transport coefficients in the quark gluon medium, like the viscosities and conductivities, and study their sensitivity to the off-shellness of the medium partons. Furthermore, from the interaction rate one can also deduce the transition rate $\omega(T)$ for particles in a heat bath of a given temperature T . In contradistinction to the elastic interaction rate, here both scattering partners are assumed to have a thermal distribution. The transition rate $\omega(T)$ is derived for the case of on- and off-shell partons by

$$\begin{aligned}\omega^{\text{on}} &= \frac{1}{n_Q^{\text{on}}} \sum_{j \in q, \bar{q}, g} \int \frac{d^3 p_Q}{(2\pi)^3} f_Q(p_Q, M_Q, T) \times \frac{1}{n_j^{\text{on}}} R_{jc}^{\text{on}}(p_Q, M_Q^i, m_j^i, M_Q^f, m_j^f), \\ \omega^{\text{off}} &= \frac{1}{n_Q^{\text{off}}} \sum_{j \in q, \bar{q}, g} \iint \frac{d^3 p_Q}{(2\pi)^3} \rho_j(m_j^{i,f}) \rho_j(M_Q^{i,f}) dm_j^{i,f} dM_Q^{i,f} f_Q(p_Q, M_Q, T) \times \frac{1}{n_j^{\text{on}}} R_{jc}^{\text{on}}(p_Q, M_Q^i, m_j^i, M_Q^f, m_j^f),\end{aligned}\quad (\text{III.8})$$

where n_j^{on} is the density of the on-shell parton j . The results for the total on- and off-shell transition rates are displayed in Fig. 4-(b). Due to the small DQPM parton widths, the influence of the spectral function is negligible and we obtain for DpQCD and IEHTL about the same transition rate $\omega_Q^{\text{off}}(T)$. Parametrizing $\omega_{q/gQ}$ by $T^{-\beta}$ we find differences between HTL-GA and DpQCD/IEHTL as discussed above. This different behaviour leads to different transport coefficients as we will show below.

IV. DRAG FORCE AND COEFFICIENT

We continue our study with the drag and diffusion coefficient. For heavy masses of c and \bar{c} quarks the relaxation times are large as compared to the typical time of an individual $qc \rightarrow qc$ and $gc \rightarrow gc$ collision. Therefore we might describe the time evolution of heavy quarks in momentum space by a Fokker-Planck (FP) equation [9, 44]:

$$\frac{\partial f(\mathbf{p}, t)}{\partial t} = \frac{\partial}{\partial p_i} [A_i(\mathbf{p}) f(\mathbf{p}, t) + \frac{\partial}{\partial p_j} (B_{ij}(\mathbf{p}) f(\mathbf{p}, t))]. \quad (\text{IV.1})$$

The drag (A) and diffusion (B) coefficients are evaluated according to [9, 13, 44] by a Kramers-Moyal power expansion of the collision integral kernel of the Boltzmann equation. Note that the diffusion tensor B admits a transverse-longitudinal decomposition (perpendicular and along the direction of the heavy quark in the frame where the fluid is at rest) and contains two independent coefficient B_{\parallel} and B_{\perp} . As realized in Refs. [13, 45], the asymptotic distribution coming out of the FP evolution deviates from a (relativistic) Maxwell-Boltzmann distribution, which is a consequence of the truncation of the Kramers-Moyal series.

A. Drag coefficient for on-shell partons

The drag coefficient A describes the time evolution of the mean momentum of the heavy quark. For on-shell partons it has been defined in the plasma rest frame by Svetitsky [9, 44]. It is obtained by multiplying (I.1) by M_Q/E_p , using for \mathcal{X} the longitudinal component of the momentum transfer, $\mathcal{X} = (p - p')^l$.

In the absence of diffusion, ($B_{ij} = 0$), the Fokker Planck equation (IV.1) allows to write

$$\frac{\partial f}{\partial t} = \frac{\partial}{\partial p_i} (A_i f) \rightarrow \frac{d \langle p_i \rangle_f}{dt} = - \int d^3 p A_i(\mathbf{p}) f(\mathbf{p}, t). \quad (\text{IV.2})$$

In particular, assuming $f = \delta(\mathbf{p} - \mathbf{p}_0)$, we obtain

$$\frac{dp_{0,i}}{dt} = -A_i(\mathbf{p}_0) \rightarrow \frac{dp_{0,i}}{d\tau} = -\frac{E_p}{M_Q} A_i(\mathbf{p}_0) \equiv \mathcal{A}_i(\mathbf{p}_0), \quad (\text{IV.3})$$

where τ is the time measured in the heavy-quark rest system. $\mathcal{A}^i = \frac{E_p}{M_Q} A^i(\mathbf{p})$ is the spatial part of the covariant \mathcal{A}^μ

$$\mathcal{A}^\mu = - \sum_{q,g} \frac{1}{2M_Q} \int \frac{d^3 q}{(2\pi)^3 2E_q} f(\mathbf{q}) a^\mu(\mathbf{p}, \mathbf{q}) \quad (\text{IV.4})$$

with

$$a^\mu(\mathbf{p}, \mathbf{q}) := \frac{1}{(2\pi)^2} \int \frac{d^3 q'}{2E_{q'}} \int \frac{d^3 p'}{2E_{p'}} (q - q')^\mu \delta^{(4)}(P_{in} - P_{fin}) \frac{1}{g_p g_Q} \sum_{k,l} |\mathcal{M}_{2,2}(p, q; i, j | p', q'; k, l)|^2 \quad (\text{IV.5})$$

using $(p - p')^\mu = -(q - q')^\mu$. We evaluate a^μ in the c.m. frame as

$$\begin{aligned} a_{cm}^\mu(\mathbf{p}_{cm}) &:= \frac{1}{(2\pi)^2} \int \frac{d^3 q'}{2E_{q'}} \int \frac{d^3 p'}{2E_{p'}} (q - q')^\mu \delta^{(3)}(\mathbf{q}' - \mathbf{p}') \delta(\sqrt{s} - \sqrt{m_q^2 + q'^2} - \sqrt{m_Q^2 + q'^2}) \frac{1}{g_p g_Q} \sum_{k,l} |\mathcal{M}_{2,2}(p, q; i, j | p', q'; k, l)|^2. \\ &= \frac{1}{(2\pi)^2} \int \frac{d^3 q'}{2E_{q'} 2E_{p'}} (q - q')^\mu \frac{E_{q'} E_{p'}}{\sqrt{s} p_{cm}} \delta(|\mathbf{q}'| - |\mathbf{p}_{cm}|) \frac{1}{g_p g_Q} \sum_{k,l} |\mathcal{M}_{2,2}(p, q; i, j | p', q'; k, l)|^2. \\ &= \frac{1}{(2\pi)^2} \frac{p_{cm}^2}{4\sqrt{s}} \int \int d\Omega_{q'} (\hat{q}_{cm} - \hat{q}'_{cm})^\mu \frac{1}{g_p g_Q} \sum_{k,l} |\mathcal{M}_{2,2}(p, q; i, j | p', q'; k, l)|^2, \end{aligned} \quad (\text{IV.6})$$

where $E_{p'} = \sqrt{M_Q^2 + p_{cm}^2}$, $E_{q'} = \sqrt{m_q^2 + p_{cm}^2}$. $\hat{\mathbf{q}}_{cm}$ is the unit vector in the direction of \mathbf{q} which we choose to have only a z component and $\hat{\mathbf{q}}'_{cm}$ is the unit vector in the direction of \mathbf{q}' with a z and a x component; $q_{cm}^0 = q_{cm}'^0$. Therefore we find

$$(\hat{q}_{cm} - \hat{q}'_{cm})^\mu = \begin{pmatrix} 0 \\ -\sin \theta \\ 0 \\ 1 - \cos \theta \end{pmatrix}. \quad (\text{IV.7})$$

The integration over the transverse component of $\hat{\mathbf{q}}'$ gives zero and we are left with a four-vector in which only the z component differs from zero. Using $1 - \cos \theta = -t/(2p_{cm}^2)$ (with θ denoting the angle between \mathbf{q} and \mathbf{q}' in the c.m. frame) we can replace the $\cos \theta$ integration by an integration over t and obtain

$$a_{cm}^0 = 0, \quad \mathbf{a}_{cm} = \frac{p_{cm}^2(s) m_1(s)}{4\pi\sqrt{s}} \times \hat{\mathbf{q}}_{cm}, \quad \text{with: } m_1(s) := \frac{1}{8p_{cm}^4} \int_{-4p_{cm}^2}^0 \sum |\mathcal{M}|^2(s, t) (-t) dt. \quad (\text{IV.8})$$

We have to calculate now \mathcal{A}^μ in the heavy quark rest frame. For this we have to boost a_{cm}^μ to this system. Using $\gamma = \frac{M_Q + E_q}{\sqrt{s}}$ and $\gamma \boldsymbol{\beta} = \frac{\mathbf{q}_{rest}}{\sqrt{s}}$, with $E_q(\mathbf{q}_{rest})$ being the energy (momentum) of the light quark in the heavy quark rest system we find

$$a_{rest}^\mu = \frac{p_{cm}^2(s) m_1(s)}{4\pi s} \begin{pmatrix} q_{rest} \\ (E_q + M_Q) \hat{\mathbf{q}}_{cm} \end{pmatrix}. \quad (\text{IV.9})$$

By construction \mathbf{p}_{rest} has the same direction as $\hat{\mathbf{q}}_{cm}$. To calculate

$$\mathcal{A}_{rest}^\mu = - \frac{1}{8(2\pi)^4 M_Q} \int \frac{p_{cm}^2(s) m_1(s)}{s} \left[\int d\Omega_{\mathbf{q}} (q \delta^{\mu 0} + (E_q + M_Q) \hat{q}_{cm}^i \delta^{\mu i}) f_r(\mathbf{q}) \right] \frac{q^2 dq}{E_q}, \quad (\text{IV.10})$$

we need $f_r(\mathbf{q})$, the invariant distribution of the light quark in the rest frame of the heavy quark. The heat bath velocity in the heavy quark rest system is given by $\mathbf{u} \equiv (u^0, \mathbf{u}) = (E_p/M_Q, -\mathbf{p}/M_Q)$. If we define $f(E_q/T)$ as the invariant distribution in the rest system of the heat bath, the light quark distribution in the heavy quark rest system is given by $f_r\left(\frac{u^0 E_q - \mathbf{u} \cdot \mathbf{q} \cos \theta_r}{T}\right)$ with θ_r denoting the angle between \mathbf{q} and \mathbf{u} (see eq. (III.4)). The expression (IV.10) then becomes

$$\mathcal{A}_{rest}^\mu = -\frac{1}{4(2\pi)^3 M_Q} \int \frac{p_{cm}^2(s) m_1(s)}{s} \left[q f_0(q) \delta^{\mu 0} + (E_q + M_Q) f_1(q) \delta^{\mu i} (\hat{u})_i \right] \frac{q^2 dq}{E_q} = \begin{pmatrix} A_{rest}^0 \\ (A_{rest}^v \hat{u})^i \end{pmatrix}, \quad (\text{IV.11})$$

where

$$f_0(q) = \frac{1}{2} \int d\cos\theta_r f\left(\frac{u^0 E_q - u q \cos\theta_r}{T}\right), \quad f_1(q) = \frac{1}{2} \int d\cos\theta_r f\left(\frac{u^0 E_q - u q \cos\theta_r}{T}\right) \cos\theta_r. \quad (\text{IV.12})$$

Using $p_{cm}^2 = \frac{q^2 M_Q^2}{s}$, A_{rest}^0 and A_{rest}^v reduce to a one dimensional integral:

$$A_{rest}^0 = \frac{M_Q}{4(2\pi)^3} \int_0^\infty \frac{q^5 m_1(s) f_0(q)}{s^2 E_q} dq, \quad A_{rest}^v = \frac{M_Q}{4(2\pi)^3} \int_0^\infty \frac{q^4 (M_Q + E_q) m_1(s) f_1(q)}{s^2 E_q} dq. \quad (\text{IV.13})$$

We note in passing that $A_{rest}^0 \rightarrow 0$ as $u \rightarrow 0$ so that A_{rest}^0 dominates A_{rest}^v for small heavy quark momenta. For $p \rightarrow +\infty$, one observes the opposite trend.

$\mathcal{A}_{\text{heat bath}}^\mu$ in the heat bath rest frame is obtained by a Lorentz transformation ($\gamma_u \boldsymbol{\beta}_u = \mathbf{p}/M_Q$, $\gamma_u = E_p/M_Q$)

$$\mathcal{A}_{\text{heat bath}}^\mu = \begin{pmatrix} \frac{E_p}{M_Q} A_{rest}^0 - A_{rest}^v \frac{\mathbf{p}}{M_Q} \cdot \hat{\mathbf{p}} \\ \frac{E_p}{M_Q} A_{rest}^v - A_{rest}^0 \frac{\mathbf{p}}{M_Q} \cdot \hat{\mathbf{p}} \end{pmatrix}. \quad (\text{IV.14})$$

which yields for the drag force in the heat bath rest frame

$$\frac{d\langle \mathbf{p} \rangle}{dt} = \mathbf{A}_{\text{heat bath}} = \frac{M_Q}{E_p} \mathcal{A}_{\text{heat bath}} = \left(A_{rest}^v - \frac{\mathbf{p} \cdot \hat{\mathbf{p}}}{E_p} A_{rest}^0 \right) \hat{\mathbf{p}}, \quad (\text{IV.15})$$

and for the energy component

$$\frac{d\langle E \rangle}{dt} = A_{\text{heat bath}}^0 = \frac{M_Q}{E_p} \mathcal{A}_{\text{heat bath}}^0 = A_{rest}^0 - \frac{\mathbf{p} \cdot \hat{\mathbf{p}}}{E_p} A_{rest}^v. \quad (\text{IV.16})$$

B. Drag coefficient for off-shell partons

For the off-shell drag force, A_i^{off} , we apply eq.(I.5) and find:

$$\mathbf{A}_{\text{heat bath}}^{\text{off}} = \left(A_{rest}^{v,\text{off}} - \tilde{A}_{rest}^{0,\text{off}} \right) \hat{\mathbf{p}}, \quad (\text{IV.17})$$

where $A_{rest}^{v,\text{off}}$ and $\tilde{A}_{rest}^{0,\text{off}}$ are defined by

$$\begin{aligned} \tilde{A}_{rest}^{0,\text{off}} &= \frac{4}{(2\pi)^7} \Pi_{i \in p,q,p',q'} \int \frac{p}{E_p} m_i dm_i \rho_i^{\text{WB}}(m_i) \int_0^\infty \frac{q^5 m_1(s) f_0(q)}{s^2 E_q} dq, \\ A_{rest}^{v,\text{off}} &= \frac{4}{(2\pi)^7} \Pi_{i \in p,q,p',q'} \int m_p m_i dm_i \rho_i^{\text{WB}}(m_i) \int_0^\infty \frac{q^4 (M_Q + E_q) m_1(s) f_1(q)}{s^2 E_q} dq. \end{aligned} \quad (\text{IV.18})$$

The details are relegated to appendix B.

C. Results

We discuss now the drag coefficients for the models HTL-GA, DpQCD and IEHTL from Ref. [28]. Here we extend the study from Ref. [28] and consider finite light quark and gluon masses in HTL-GA model for a running coupling α . In the DpQCD approach, the light and heavy quark and gluon masses are given by the DQPM pole masses. Fig. 5-(a) shows the drag coefficient (IV.15) and (IV.17) of heavy quarks as a function of the heavy quark momentum. We display the results for the HTL-GA model for a constant and a running α and for massless and massive light quarks and gluons, where $m_{q,g}^{HTL}$ denote the light quark and gluon mass given by HTL and plotted in figure 2-(a). The temperature of the heat bath is chosen as $T = 2T_c$. In the HTL-GA approach a finite mass of the light quark leads to a reduction of the drag coefficient for a given temperature. This effect is similar for both, the constant and running coupling. However, the reduction of the drag coefficient is not uniform as a function of p_Q and dominantly affects the largest momentum. The drag coefficient in the DpQCD model is in between the extremes of the HTL-GA approach.

Figure 5-(a) illustrates also the influence of a finite parton width on the heavy quark drag coefficient, where the drag coefficient is displayed for on-shell partons (DpQCD) and off-shell partons (IEHTL) as a function of the heavy quark momentum and for a temperature of $2T_c$. For off-shell partons the drag coefficient is slightly lower than for the corresponding on-shell case. We see in Fig. 5-(a) that for thermal heavy quark $p_Q \sim 2$ GeV the IEHTL and the on-shell DpQCD give a drag coefficient which is slightly above the one from the HTL-GA drag coefficient for a fixed α . For a running coupling in HTL-GA the drag coefficient (IV.15) is about a factor of 2.5 larger.

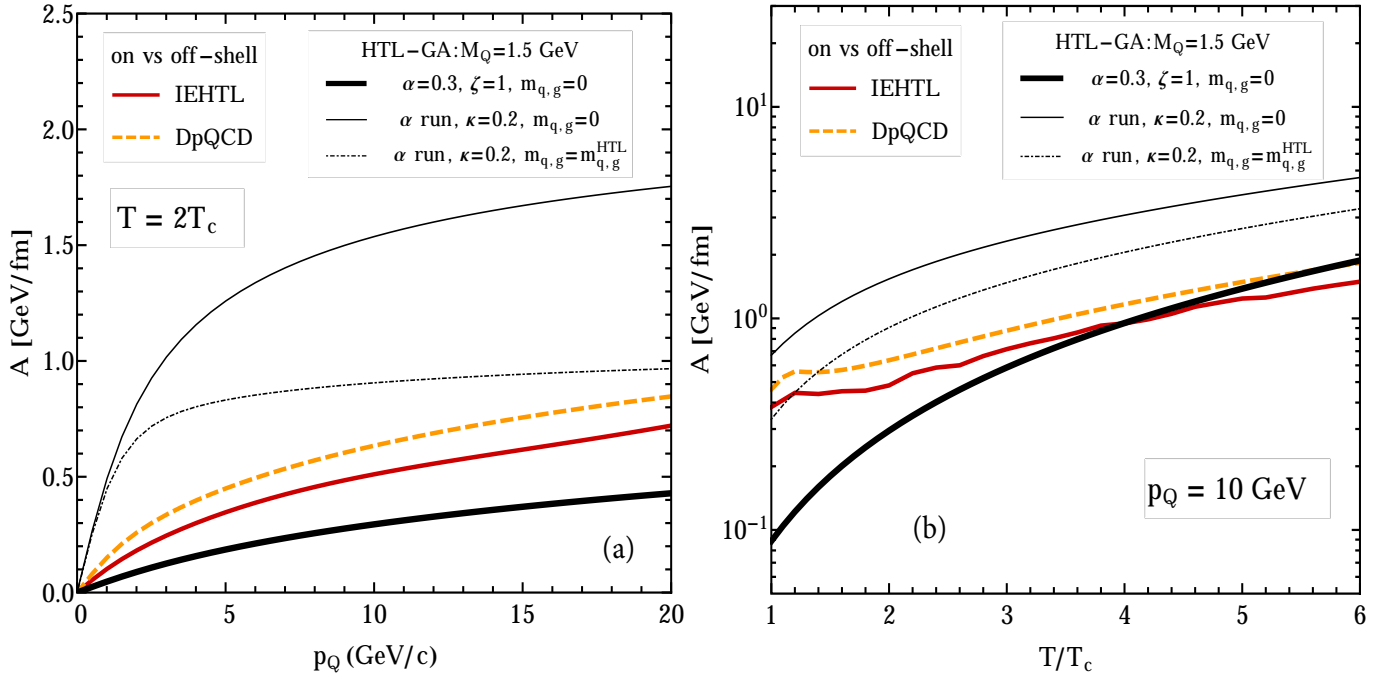


FIG. 5. (Color online) The drag coefficient A of c -quarks in the plasma rest frame (IV.15) and (IV.17) for the three different approaches as a function of the heavy quark momentum p_Q for $T = 2T_c$ (a) and as a function of the temperature T/T_c ($T_c = 0.158$ GeV) for an intermediate heavy quark momentum, $p_Q = 10$ GeV (b).

In order to understand the reduction of the drag coefficient in the HTL-GA and DpQCD/IEHTL approaches, we plot in Fig. 5-(b) the drag coefficient as a function of the temperature for an intermediate (10 GeV/c) heavy quark momentum. From the temperature dependence of the drag coefficient in the HTL-GA model with massless/massive light quarks and gluons, one sees that the ratio $A(\text{massive } q,g)/A(\text{massless } q,g)$ shows almost no dependence on the temperature. Comparing the different results, one notices that in the HTL-GA model the drag is always increasing as a function of the temperature whereas for the DpQCD/IEHTL models we observe a minimum at $1-2 T_c$. The bump observed around $1-2 T_c$ is directly related to the temperature dependence of the DQPM parton masses. The large drag at low temperatures in DpQCD/IEHTL is due to the strong increase of the running coupling (infrared enhancement) at these temperatures.

In the HTL-GA model (with massless partons) an increasing temperature increases the density of scattering partners in the QGP $f \propto \exp(-\frac{\sqrt{q^2}}{T})$. For quarks with zero mass this increase is $\propto T^3$ what is partially counterbalanced by the decrease of the cross section $\propto T^{-2}$. In the DpQCD/IEHTL approaches we have in addition to take into account that the light quark masses and the

coupling constants increase with temperature. This lowers on the one side the increase of the parton density ($f \propto \exp(-\frac{\sqrt{m_{q,g}^2 + q^2}}{T})$) with temperature, allows on the other side for a larger momentum transfer in a single collision. The drag coefficient increases with the heavy quark momentum for both, the HTL-GA and DpQCD/IEHTL model. The running coupling in HTL-GA leads to larger values of the heavy quark drag coefficient. The difference of A between the HTL-GA and DpQCD/IEHTL models is on one side due to the different masses and on the other side due to the fundamental ingredients used in the corresponding cross sections, i.e. the coupling and the infrared regulator [28] as explained above. The low temperature enhancement of DpQCD/IEHTL as compared to HTL-GA is essentially due to the strong increase of the coupling $\alpha(T/T_c)$ for temperatures close to T_c .

The drag coefficient A for the DpQCD/IEHTL models can be parametrized as a function of p_Q by the functional form $A(p_Q) = ap_Q - bp_Q^2 + cp_Q^3 - dp_Q^4$, where a is the dominant coefficient. For $A^{T=T_c}(p_Q) = 0.03609p_Q - 0.00146p_Q^2 + 0.000037p_Q^3 - 5.469 \times 10^{-7}p_Q^4$.

It is interesting to compare the drag coefficient with the collision rates (figs.3-(a) and (b)). The ratio of both is proportional to the average longitudinal momentum change in a single collision $\langle \Delta p_L \rangle \propto A/\text{Rate}$, where A and the rate are defined in eqs. (I.1) and (I.5), respectively. $\langle \Delta p_L \rangle$ is illustrated in Fig. 6 as a function of the heavy quark momentum (a) and as a function of the temperature (b). Whereas the heavy quark drag coefficient and the heavy quark rate are larger for the HTL-GA model with running α , the longitudinal momentum transfer per collision $\langle \Delta p_L \rangle$ is smaller as compared to the DpQCD/IEHTL models because a running $\alpha(Q^2)$ in HTL-GA favors collisions with a small momentum transfer. For large momenta and for a running α $\langle \Delta p_L \rangle$ becomes almost independent of the incoming momentum. In the DpQCD/IEHTL models (with a temperature dependent coupling) as well as in HTL-GA with a fixed coupling $\langle \Delta p_L \rangle$ increases with p_Q . Off-shell and on-shell approaches show an almost identical $\langle \Delta p_L \rangle$ per collision such that the differences in the drag coefficient are only due to different rates. If one regards the temperature dependence one sees that the increasing coupling in DpQCD/IEHTL is almost completely counterbalanced by the increasing mass of the partons. Therefore the DpQCD/IEHTL models show only a very moderate change of $\langle \Delta p_L \rangle$ per collision which falls in between the HTL-GA approach for running and fixed coupling. Also HTL-GA with a running coupling shows only a very moderate change of $\langle \Delta p_L \rangle$ per collision as a function of the temperature. In pQCD it is known that $A \propto T^2$ and the rate $R \propto T$ [11]. Therefore $\langle \Delta p_L \rangle \propto T$ in pQCD as shown in figure 6-(b) within HTL-GA for constant α (thick black line).

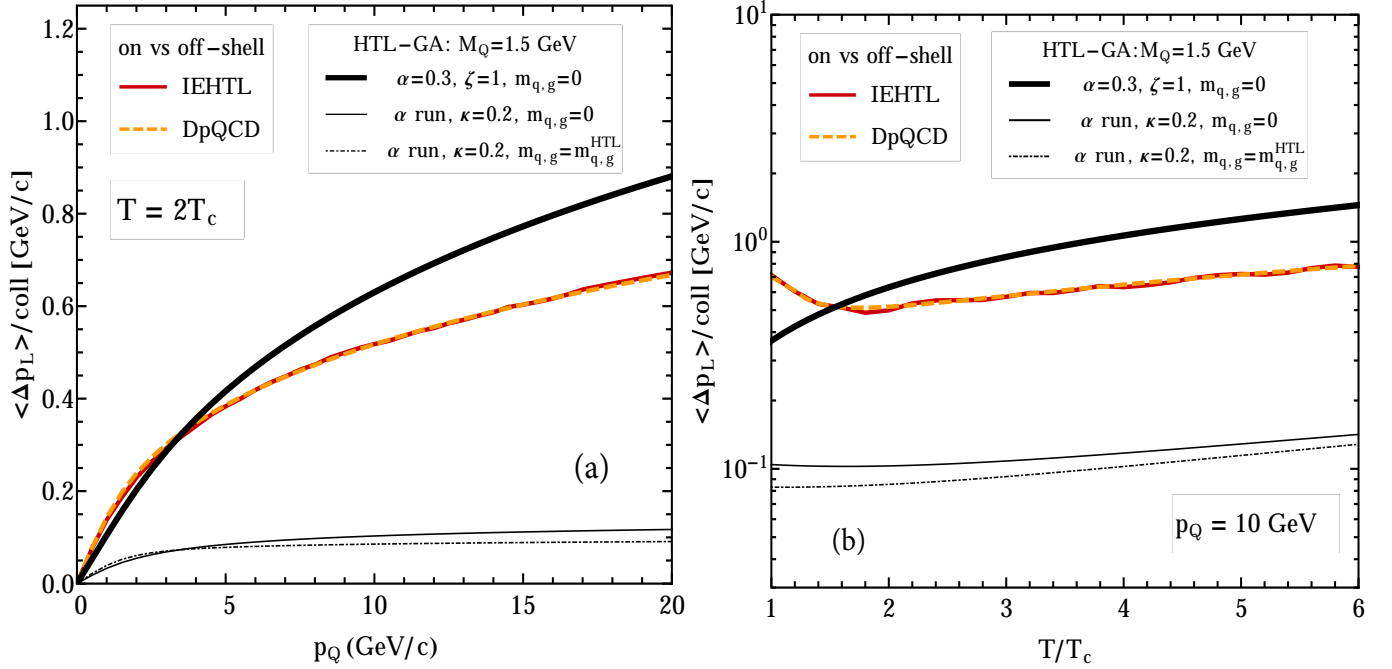


FIG. 6. (Color online) The average loss of longitudinal momentum $\langle \Delta p_L \rangle$ per collision for the three different approaches as a function of the heavy quark momentum and for $T = 2T_c$ (a) and as a function of the medium temperature T/T_c ($T_c = 0.158$ GeV) for intermediate heavy quark momentum $p_Q = 10$ GeV (b).

Comparing the massless (thin black line) and massive (dotted dashed black line) parton cases in the HTL-GA model in Figs.6-(a) and (b), one concludes that the scattering of a heavy quark on massive partons transfers less longitudinal momentum than the scattering on massless partons, except for low heavy quark momenta $p_Q \ll T$. The finite parton mass contributes to the increase of the c.m. momentum and therefore reduces the threshold and opens the phase space for the total cross section. We will discuss this now for the case of the scattering of a heavy quark on a light quark. From eq.(III.3) we find that for $p \gg M_Q$ the rate in the

rest system of the heavy quark is given by

$$\mathcal{R} \propto \frac{g_p}{8\pi^2} \frac{T}{u^0 u} \int dq \frac{q^2}{q^0} \sigma \left(\frac{q M_Q}{\sqrt{s}} \right) e^{-\frac{u^0 q^0 - uq}{T}} \quad (\text{IV.19})$$

which yields for $m_q \gg T$

$$\mathcal{R} \propto (m_q T)^{\frac{3}{2}} e^{-\frac{m_q}{T}} \sigma_{as}, \quad (\text{IV.20})$$

where σ_{as} is the asymptotic value of σ . For the drag coefficient, one gets from eq.(IV.13)

$$\mathcal{A} \propto \frac{g_p}{8\pi^2} \frac{T}{u} \int_0^{+\infty} \frac{q dq}{q^0} e^{-\frac{u^0 q^0 - uq}{T}} \times \langle \sigma |t| \rangle \quad (\text{IV.21})$$

and finds in the same limit, $m_q \gg T$,

$$\mathcal{A} \propto \sqrt{m_q T^3} \times e^{-m_q/T} \times \langle \sigma |t| \rangle_{q=\frac{m_q P}{M_Q}}. \quad (\text{IV.22})$$

Consequently, if $m_q \gg T$, both the collisions rate as well as the drag decrease with increasing mass m_q . Besides, from eqs.(IV.20) and (IV.22) one sees directly that in this regime

$$\Delta p_L \propto \mathcal{A}/\mathcal{R} \propto \frac{\langle |t| \rangle}{m_q}, \quad \text{with} \quad \langle |t| \rangle = \frac{\langle \sigma |t| \rangle_{q=\frac{m_q P}{M_Q}}}{\sigma_{as}}. \quad (\text{IV.23})$$

From eq.(IV.23) one deduces that for $m_q \gg T$, Δp_L decreases with increasing light quark mass, which explains the trends observed in Fig. 6.

From Eqs. (IV.20) and (IV.22), we conclude that the differences in the asymptotic values between the HTL-GA and DpQCD are related to the total cross section for the rate and are related to the quantity $\langle \sigma |t| \rangle = \int \frac{d\sigma}{dt} |t| dt$ for the drag coefficient. $\langle \sigma |t| \rangle$ for the elastic qQ scattering is plotted in figure 7-(b) and compared to the total cross section σ^{qQ} presented in fig.7-(a) following the models HTL-GA with α running and DpQCD. The gap in σ^{qQ} between HTL-GA and DpQCD is reduced in $\langle \sigma |t| \rangle$, which explains that the difference between HTL-GA and DpQCD is more important on the level of the rate compared to the drag coefficient.

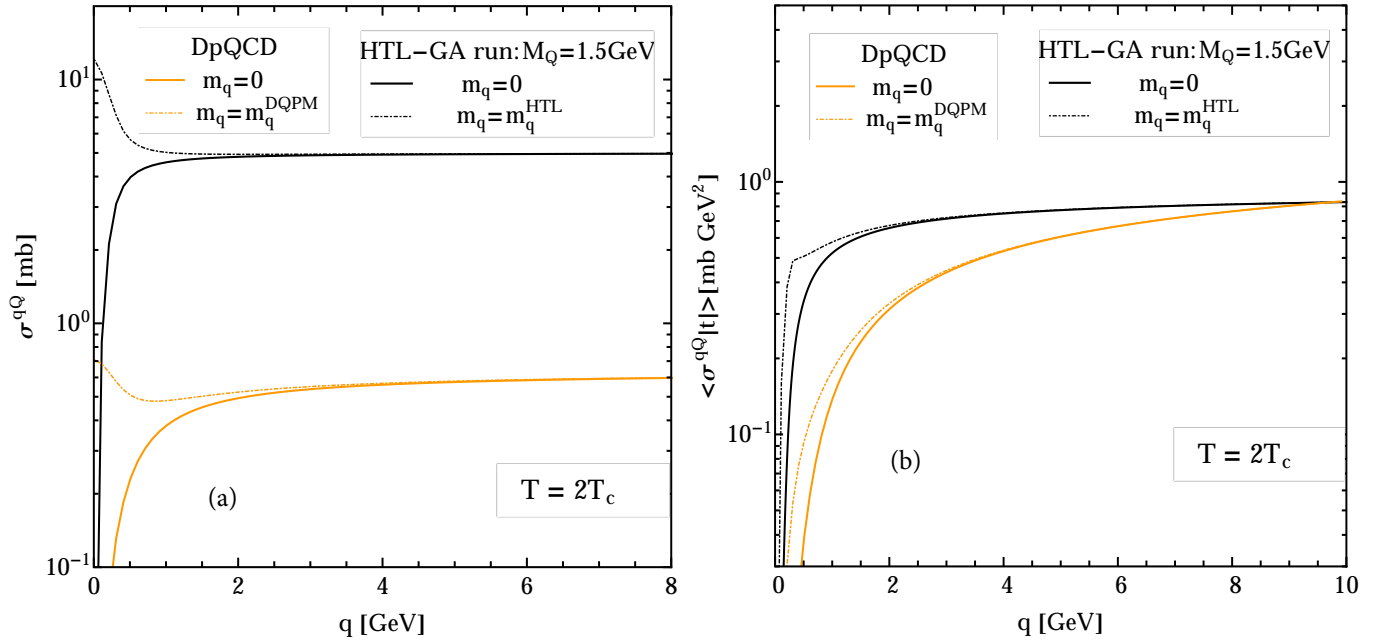


FIG. 7. (Color online) The total cross section σ^{qQ} for the elastic qQ scattering (left) and $\langle \sigma |t| \rangle = \int \frac{d\sigma}{dt} |t| dt$ for the models HTL-GA with running α and DpQCD as a function of q which is related to s by $s = M_Q^2 + m_q^2 + 2M_Q E_q$.

Figure 8 compares the results for charm quarks in our approach with other models for the coefficient η_D related to the drag coefficient by $\eta_D = A/p_Q$ at small momentum. We want to stress that due to the non-trivial p -dependence, η_D only represents the transport properties at small momentum. However, since several results for this coefficient have been presented in the literature it may serve for a comparison between different models. For all calculations we have assumed that the heavy quark interacts with a particle (light quarks and gluons) of the plasma at temperature $T = 300$ MeV and the calculations have been performed with the coupling constants of the corresponding publications. M&T refers to Moore and Teaney (equation (B.31) with $\alpha = 0.3$ of [11]), VH&R to van Hees and Rapp [10, 12, 46] (with a resonance width of 400 MeV), P&P to Peshier and Peigne [33] and AdS/CFT to the drag coefficient calculated in the framework of the anti de Sitter/conformal field theory by Gubser [47, 48]. HTL-GA (with $\alpha = 0.3$) and HTL-GA (with α run) refer to the two parameter sets of the HTL-GA model for constant and running coupling as defined in [23].

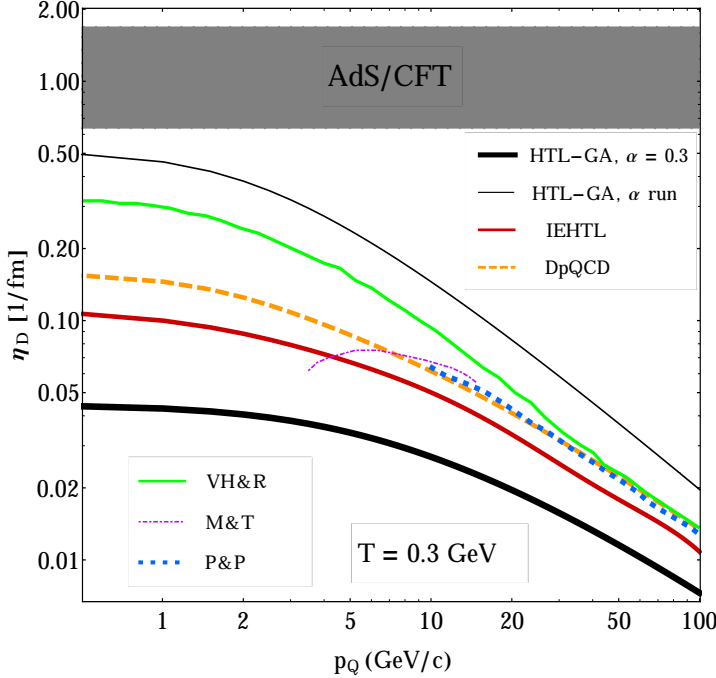


FIG. 8. (Color online) η_D , the drag coefficient A over p_Q for c -quarks for different models as a function of the heavy quark momentum. The temperature of the scattering partners is 300 MeV. M&T refers to Moore and Teaney (equation (B.31) with $\alpha = 0.3$ of [11]), VH&R to van Hees and Rapp [10, 12, 46] (with a resonance width of = 400 MeV), P&P to Peshier and Peigne [33] and AdS/CFT to the drag coefficient calculated in the framework of the anti de Sitter/conformal field theory by Gubser [47, 48]. HTL-GA (with $\alpha = 0.3$) and HTL-GA (with α run) refer to the two parameter sets of the HTL-GA model for constant and running coupling constant defined in [23].

The largest coefficient η_D is observed for the AdS/CFT approach in which η_D is momentum independent. All perturbative and non-perturbative QCD-based coefficients η_D decrease with increasing p_Q which can be interpreted by the fact that with increasing momentum the relative momentum change becomes lower. The values of η_D vary substantially due to different assumptions on the infrared regulators and couplings and due to different ingredients, like the presence of $q\bar{q}$ resonances in the plasma for the VH&R model and off-shell dressed partons for IEHTL. One may ask the question why the transverse momentum dependence of R_{AA} and v_2 , observed in heavy-ion reactions, can be reproduced by different theories despite of quite different drag coefficients. As Gossiaux et al. [20] have pointed out the drag coefficient is only one of two key ingredients in heavy-ion transport approaches. The other is the expansion of the plasma, described either by hydrodynamical equations, a (tuned) fireball model or by the parton-hadron-string dynamics (PHSD) transport approach. Therefore the measured R_{AA} and v_2 are not a direct image of η_D or the drag coefficient A .

D. Spatial diffusion coefficient

In this section we will discuss an approximate calculation of the diffusion constant in coordinate space, D_s , which is related to the coefficient η_D by $D_s = T/(M_Q \eta_D)$ [11]. This relation, defined by Moore and Teaney [11], is strictly valid only in the non-relativistic limit, i.e. for velocities $\gamma v < \alpha/\sqrt{s}$ to leading logarithm in T/m_D , where m_D is the Debye mass. Therefore it is a good approximation to model the interaction of thermal heavy quarks, $M_Q \gg T$, with a typical thermal momentum $p \sim \sqrt{MT}$ and a velocity $v \sim \sqrt{T/M} \ll 1$. Since $p \gg T$, it takes many collisions for the heavy quarks to change their momentum substantially. Even for hard collisions with a momentum transfer $q \sim T$, it takes $\sim M/T$ collisions to change the momentum by a factor of the order one. Therefore, we may model the interaction of the heavy quarks with the medium as uncorrelated momentum kicks.

Fig. 9 displays $2\pi T D_s$ for charm quarks as a function of the plasma temperature. In addition to the approaches discussed in this article, we plot also the results from quenched lattice QCD [49] for the spatial charm diffusion coefficient at finite temperature.

The spatial charm quark diffusion constant is related to the charmonium spectral function via the Kubo formula, Ref. [49]. The estimate given by IQCD for the charm diffusion coefficient is $\approx 1/\pi T$ in the range $1.5T_c \lesssim T \lesssim 3T_c$. Note that the spatial charm diffusion coefficient obtained at $1.46T_c$ is more reliable than that obtained at higher temperatures, shown in Fig. 9. At $2.20T_c$ and $2.93T_c$, due to the lack of precise information on the spectral function and also due to a smaller number of data points that can be used in the MEM analyses [49], the uncertainties of the spatial charm diffusion coefficient might be underestimated.

At first sight, Fig. 9 seems to show that all the approaches presented in our study fail to agree with the IQCD results, even if the HTL-GA with running α spatial diffusion coefficient is in the vicinity of the IQCD results. Indeed, for the models HTL-GA with constant α and for DpQCD/IEHTL the spacial diffusion coefficients D_s are very large compared to the one given by IQCD. However, one should consider this comparison with caution since, as said, the relation used to determine D_s [11] is an approximation. In the DpQCD/IEHTL model the momentum transfer in a single collision is larger than \sqrt{MT} as shown in Fig. 6. Therefore a more detailed calculation of D_s is necessary in order to arrive at a solid comparison between the IQCD result and our different approaches. Such a calculation, however, is beyond the scope of this study.

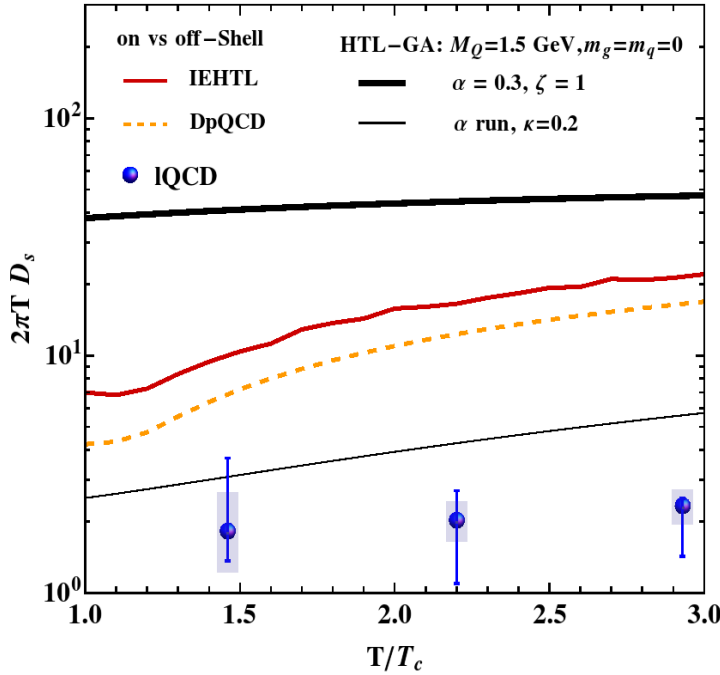


FIG. 9. (Color online) The spatial diffusion coefficient D_s for c -quarks, for HTL-GA with constant and running coupling [23], for DpQCD/IEHTL in comparison with the results from IQCD [49] as a function of the temperature. For the IQCD points the boxes show the statistical error estimated by the 'Jackknife method' while the bars stand for systematic uncertainties from the MEM analyses.

V. DYNAMICAL COLLISIONAL ENERGY LOSS

The collisional energy loss dE/dt has been formulated by Bjorken (I.1) and is calculated in Sec.IV eq. (IV.16). Similar to the drag coefficient the collisional energy loss for on-shell partons eq.(IV.16) can be easily extended for the off-shell case using (I.4). Going through similar calculations we arrive at

$$\frac{dE^{\text{off}}}{dt}(T) = \left(A_{\text{rest}}^{0,\text{off}} - \tilde{A}_{\text{rest}}^{\text{v,off}} \right) \hat{p}, \quad (\text{V.1})$$

where $A_{\text{rest}}^{0,\text{off}}$ and $\tilde{A}_{\text{rest}}^{0,\text{off}}$ are defined by

$$\begin{aligned} A_{\text{rest}}^{0,\text{off}} &= \frac{4}{(2\pi)^7} \Pi_{i \in p,q,p',q'} \int m_p m_i dm_i \rho_i^{\text{WB}}(m_i) \int_0^\infty \frac{q^5 m_1(s) f_0(q)}{s^2 E_q} dq, \\ \tilde{A}_{\text{rest}}^{\text{v,off}} &= \frac{4}{(2\pi)^7} \Pi_{i \in p,q,p',q'} \int \frac{p m_p}{E_p} m_i dm_i \rho_i^{\text{WB}}(m_i) \int_0^\infty \frac{q^4 (M_Q + E_q) m_1(s) f_1(q)}{s^2 E_q} dq. \end{aligned} \quad (\text{V.2})$$

More details are given in the appendix C. The heavy quark energy loss (eq.IV.16) (as a function of the heavy quark momentum) is illustrated in Fig. 10-(a) for the HTL-GA model for a constant and for a running α and for massless and massive light quarks and gluons. The conclusions we have drawn for the drag coefficient remain also valid for the collisional energy loss, especially concerning the reduction of dE/dx for finite light quark masses in the HTL-GA model for a given temperature. The running coupling leads to more energy loss in the HTL-GA approach. Fig 10-(b) shows that with increasing temperature - which corresponds to the increase of the parton masses in the DpQCD/IEHTL and the massive HTL-GA models- the energy loss becomes larger. This is more pronounced for large heavy quark momenta. dE/dx can be linked to the drag coefficient by

$$\frac{d\langle E \rangle}{dt} = \beta \cdot \frac{d\langle \mathbf{p} \rangle}{dt} + (1 - \beta^2) A_{rest}^0, \quad (\text{V.3})$$

where the second term $(1 - \beta^2) A_{rest}^0$ corresponds to a gain from the medium to arrive at the average energy in the heat bath. This gain is seen in Fig. 10-(a) for small heavy quark momenta where dE/dx is negative.

The temperature dependence of the collisional energy loss for an intermediate heavy quark momentum ($p_Q = 10$ GeV/c) is displayed in Fig. 10-(b) for the HTL-GA model with massless/massive light quarks and gluons and for the DpQCD/IEHTL models. The ratio $\frac{dE}{dx}(\text{massive } q, g) / \frac{dE}{dx}(\text{massless } q, g)$ shows almost no temperature dependence in the HTL-GA model. Fig. 10-(b) shows that the energy loss is increasing as a function of the temperature for both, the HTL-GA and DpQCD/IEHTL models. For low heavy quark momenta and higher medium temperatures, the heavy quark loses less energy by elastic collisions. At low momentum heavy quarks start to gain energy to approach thermal equilibrium.

Fig. 10-(a) and (b) quantify also the influence of the finite parton mass and width on the heavy quark collisional energy loss. Massive heavy quark scattering on massless partons, described by the HTL-GA approach (with α running), loose more energy as compared to the scattering on massive partons. Comparing the DpQCD and IEHTL models, one deduces that the energy loss for partons with finite width is smaller as for the corresponding on shell particles. This difference becomes more important with increasing p_Q . The large dE/dx at low temperature observed in DpQCD/IEHTL is again due to the strong increase of the coupling.

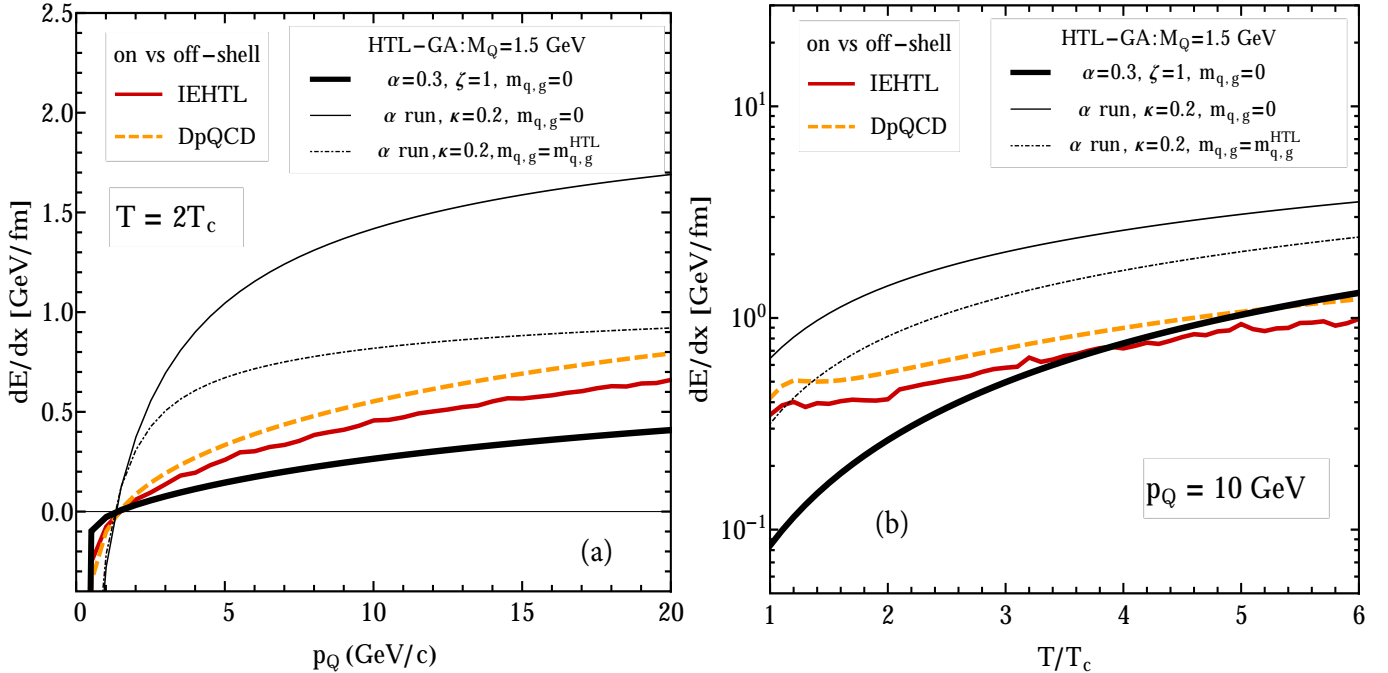


FIG. 10. (Color online) c -quark energy loss, dE/dx , in the plasma rest frame from the three different approaches as a function of the heavy quark momentum p_Q for $T = 2T_c$ ($T_c = 0.158$ GeV) (a) and as a function of the medium temperature T for a heavy quark momentum of $p_Q = 10$ GeV (b). The heavy quark mass and momentum are given in GeV.

VI. DIFFUSION COEFFICIENT AND TRANSVERSE MOMENTUM FLUCTUATIONS \hat{q}

The covariant diffusion coefficient $\mathcal{B}^{\mu\nu} = \frac{E_p}{M_Q} B^{\mu\nu}(\mathbf{p})$ has a tensorial structure and is given by the explicit expression

$$\mathcal{B}^{\mu\nu}(\mathbf{p}) = \frac{E_p}{M_Q} \frac{1}{2} \langle (p-p')^\mu (p-p')^\nu \rangle = \frac{1}{2(2\pi)^5 M_Q} \int \frac{d^3 q}{2E_q} f(\mathbf{p}) b^{\mu\nu}(\mathbf{p}),$$

$$\text{with: } b^{\mu\nu}(\mathbf{p}) := \int \frac{d^3 q'}{2E_{q'}} \int \frac{d^3 p'}{2E_{p'}} \frac{(p-p')^\mu (p-p')^\nu}{2} \delta^{(4)}(P_{in} - P_{fin}) \frac{1}{g_p g_Q} \sum_{k,l} |\mathcal{M}_{2,2}^{\text{off}}(p, q; i, j | p', q'; k, l)|^2(s, t). \quad (\text{VI.1})$$

Using the projection in longitudinal and transverse direction (with respect to the incoming momentum \mathbf{p})

$$(\hat{\Pi}_L(\mathbf{p}))_{ij} := \frac{p_i p_j}{p^2}, \quad (\hat{\Pi}_T(\mathbf{p}))_{ij} := I_{ij} - \frac{p_i p_j}{p^2}. \quad (\text{VI.2})$$

where $\hat{\Pi}_L$ and $\hat{\Pi}_T$ are the projectors along \mathbf{p} and perpendicular to \mathbf{p} , respectively, the spatial part of the diffusion coefficient $B^{ij}(\mathbf{p})$ can be decomposed into a longitudinal and a transverse component,

$$B^{ij}(\mathbf{p}) = B_L(p) \hat{p}^i \hat{p}^j + B_T(p) (\delta^{ij} - \hat{p}^i \hat{p}^j)$$

$$\text{with: } B_L(p) = \frac{1}{2} \frac{\Delta \langle p_L^2 \rangle}{\Delta t} := \text{tr}(B \cdot \hat{\Pi}_L(\mathbf{p})); \quad B_T = \frac{1}{4} \frac{\Delta \langle p_T^2 \rangle}{\Delta t} := \frac{1}{2} \text{tr}(B \cdot \hat{\Pi}_T(\mathbf{p})), \quad (\text{VI.3})$$

where $\langle \Delta p_L^2 \rangle$ ($\langle \Delta p_T^2 \rangle$) is the longitudinal (transverse) averaged squared momentum acquired by the heavy quark in a single collision with the medium constituents during its propagation through the plasma. The coefficients B_L and B_T measure the second moment of the longitudinal and transverse momentum distribution of the heavy quark. $\langle \Delta p_T \rangle = 0$ and $\langle \Delta p_L \rangle$ have been studied in Sec. IV. The transverse second moment B_T is related to \hat{q} which is defined as the average squared transverse momentum gain per unit length by [23, 50]:

$$\hat{q} = \frac{\Delta \langle p_T^2 \rangle}{\Delta x} = \frac{\langle p_T^2 \rangle_{\text{single coll}}}{\ell} = \frac{4E_Q}{p_Q} B_T. \quad (\text{VI.4})$$

\hat{q} quantifies the increase of the variance $\langle p_T^2 \rangle$ per unit length during the heavy quark propagation. In the following we will present \hat{q} for massless/massive on-shell and off-shell partons.

A. \hat{q} for on-shell partons

For massive on-shell partons \hat{q} is given by:

$$\hat{q}^{\text{on}}(p) = \frac{M_Q^3}{2(2\pi)^3 p_Q} \int_0^{+\infty} \frac{q^5}{s^2 E_q} \left[\frac{m_1^{\text{on}}(s) - m_2^{\text{on}}(s)}{2} (f_0 + f_2) + \frac{(E_q + M_Q)^2}{s} m_2^{\text{on}}(s) (f_0 - f_2) \right] dq \quad (\text{VI.5})$$

with:

$$m_1^{\text{on}}(s) = \int_{-1}^1 d\cos\theta \frac{1 - \cos\theta}{2} \sum |\mathcal{M}^{\text{on}}|^2 = \frac{1}{8p_{cm}^4} \int_{-4p_{cm}^2}^0 \sum |\mathcal{M}^{\text{on}}|^2(s, t) \times (-t) dt$$

$$m_2^{\text{on}}(s) = \int_{-1}^1 d\cos\theta \left(\frac{1 - \cos\theta}{2} \right)^2 \sum |\mathcal{M}^{\text{on}}|^2 = \frac{1}{32p_{cm}^6} \int_{-4p_{cm}^2}^0 \sum |\mathcal{M}^{\text{on}}|^2(s, t) t^2 dt, \quad (\text{VI.6})$$

and:

$$f_i = \frac{1}{2} \int d\cos\theta f \left(\frac{u^0 E_q - u q \cos\theta}{T} \right) \cos^i \theta, \quad i \in [0, 1, 2]. \quad (\text{VI.7})$$

The details are given in the appendix D.

B. \hat{q} for off-shell partons

The off-shell \hat{q}^{off} (using the Breit-Wigner spectral functions for the off-shell partons) is deduced by extending the on-shell \hat{q}^{on} as

$$\hat{q}^{\text{off}}(p) = \frac{1}{2(2\pi)^3} \Pi_{i \in p, q, p', q'} \int \frac{m_p^2}{p_Q} m_i dm_i \rho_p^{\text{WB}}(m_i) \int \frac{q^5 m_p}{s^2 E_q} \left[\frac{m_1^{\text{off}}(s) - m_2^{\text{off}}(s)}{2} (f_0 + f_2) + \frac{(E_q + m_p)^2}{s} m_2^{\text{off}}(s) (f_0 - f_2) \right] dq \quad (\text{VI.8})$$

with:

$$m_1^{\text{off}}(s) = \int_{-1}^1 d\cos\theta \frac{1 - \cos\theta}{2} \sum |\mathcal{M}^{\text{off}}|^2 = \frac{1}{4p_Q^i p_Q^f} \int_{t_{\min}}^{t_{\max}} \sum |\mathcal{M}^{\text{off}}|^2(s, t) \left[1 - \frac{t - (M_Q^i)^2 + (M_Q^f)^2 - 2E_Q^i E_Q^f}{2p_Q^i p_Q^f} \right] dt \quad (\text{VI.9})$$

$$m_2^{\text{off}}(s) = \int_{-1}^1 d\cos\theta \left(\frac{1 - \cos\theta}{2} \right)^2 \sum |\mathcal{M}^{\text{off}}|^2 = \frac{1}{8p_Q^i p_Q^f} \int_{t_{\min}}^{t_{\max}} \sum |\mathcal{M}^{\text{off}}|^2(s, t) \left[1 - \frac{t - (M_Q^i)^2 + (M_Q^f)^2 - 2E_Q^i E_Q^f}{2p_Q^i p_Q^f} \right]^2 dt,$$

where p_Q^i (M_Q^i) is the initial heavy momentum (mass) and p_Q^f (M_Q^f) is the final heavy momentum (mass). Fig. 11-(a) and (b) compare \hat{q} for the on- and off-shell calculations as a function of the heavy quark momentum and of the medium temperature, respectively. The results for the HTL-GA model are given for constant or running α and for massless/massive light quarks and gluons. These figures give also the corresponding \hat{q} for the DpQCD/IEHTL approaches. For all the models, after a minimum at $p_Q \in [1, 2]$ GeV, \hat{q} increases as a function of the heavy quark momentum. Heavy quarks which collide with the running α in the HTL-GA approach show a much larger transverse momentum transfer per unit length as compared to calculations with a constant coupling which does not depend on the momentum transfer. The calculations in the HTL-GA approach (with a fixed coupling) and in the DpQCD approach (with a temperature dependent coupling) show a similar \hat{q} above $T = 6T_c$ but differ largely for temperatures close to T_c . Employing a spectral function lowers the transverse momentum transfer by about 20% independent of momentum or temperature.

We find that \hat{q} decreases with increasing the mass of the light partons and gluons. As for the drag coefficient, a system with massless quarks has a shorter mean-free-path than one with massive partons. This is not compensated by a larger momentum transfer in an individual collision if the partons carry a mass. For the case of the scattering of a heavy quark on a light quark we find from eq.(VI.5) that for $p \gg M_Q$ \hat{q} in the rest system of the heavy quark is given by

$$\hat{q} \propto \frac{g_p}{4\pi^2} \frac{T}{u^2} \int_0^{+\infty} \frac{q^2 dq}{q^0} e^{-\frac{u^0 q^0 - uq}{T}} \times \langle \sigma |t| \rangle \quad (\text{VI.10})$$

and find in the limit, $m_q \gg T$,

$$\hat{q} \propto (m_q T)^{3/2} \times e^{-m_q/T} \times \langle \sigma |t| \rangle_{q=\frac{m_q P}{M_Q}}. \quad (\text{VI.11})$$

Consequently, if $m_q \gg T$, \hat{q} decreases with increasing mass m_q .

The temperature dependence of \hat{q} for an intermediate (10 GeV/c) heavy quark momentum, displayed in Fig. 11-(b), shows the same form for all the models except near T_c where DpQCD/IEHTL has a slight bump related to the temperature dependence of DQPM partons masses. Fig. 11-(b) shows that at high temperatures \hat{q} increases strongly with the temperature for both, the HTL-GA and the DpQCD/IEHTL models.

As for the longitudinal momentum transfer, we study the transverse momentum transfer in a single collision, i.e. $\langle \Delta p_T^2 \rangle$ which is proportional to the ratio between \hat{q} and the interaction rate. $\langle \Delta p_T^2 \rangle$ is illustrated in Fig. 12 as a function of the heavy quark momentum (a) and as a function of the temperature (b). Whereas the heavy quark \hat{q} and the heavy quark rate are larger for the HTL-GA model with running α , the transverse momentum transfer per collision $\langle \Delta p_T^2 \rangle$ is smaller as compared to the DpQCD/IEHTL models. $\langle \Delta p_T^2 \rangle$ increases as a function of the temperature which shows that the increase of the temperature leads to more transverse momentum change and almost constant longitudinal momentum transfer, as seen in the temperature dependence of $\langle \Delta p_L \rangle$. Comparing the massless (thin black line) and massive (dotted dashed black line) parton cases in the HTL-GA model in Figs. 12-(a) and (b), one deduces that in contrast to the longitudinal momentum transfers the scattering of a heavy quark on massive partons transfers more transverse momentum than the scattering on massless partons for all heavy quark momenta. This can be seen from eqs.(IV.20) and (VI.11) where in the regime $m_q \gg T$

$$\Delta p_T^2 \propto \hat{q} / \mathcal{R} \propto \langle |t| \rangle, \quad \text{with} \quad \langle |t| \rangle = \frac{\langle \sigma |t| \rangle_{q=\frac{m_q P}{M_Q}}}{\sigma_{as}}, \quad (\text{VI.12})$$

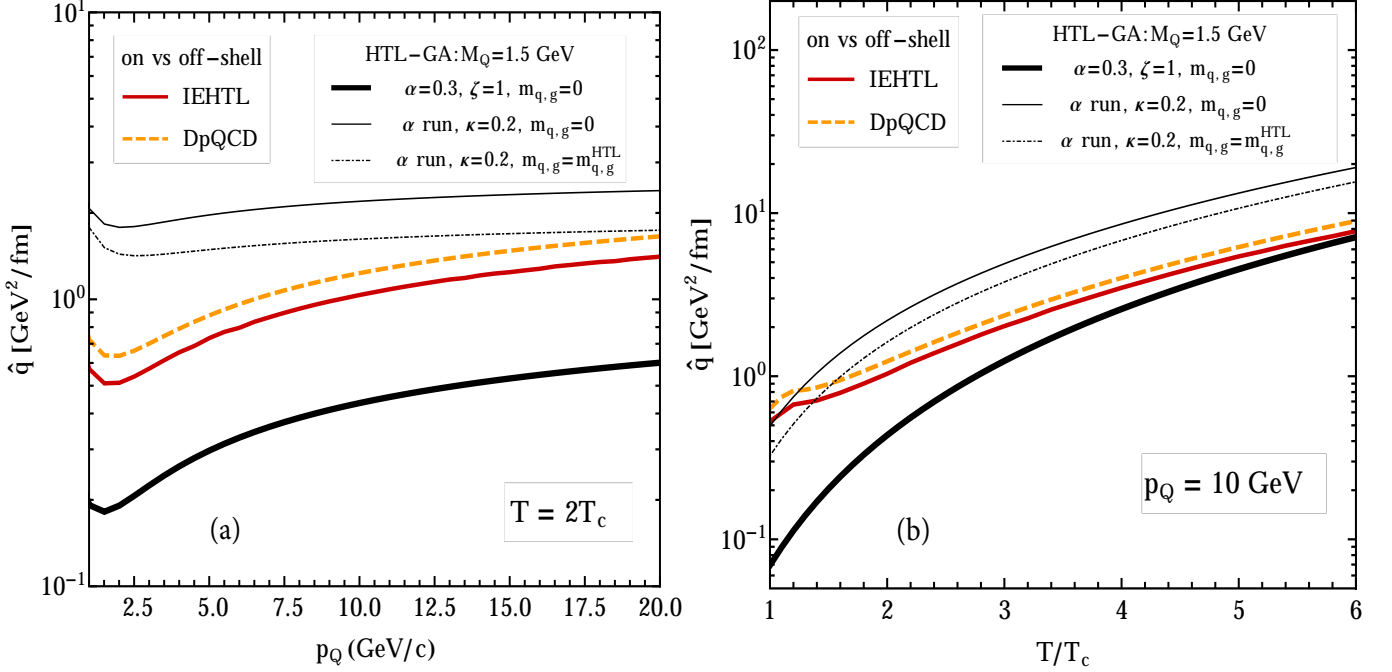


FIG. 11. (Color online) \hat{q} for c -quarks in the plasma rest frame for the three different approaches. (a) \hat{q} as a function of the heavy quark momentum p_Q for $T = 2T_c$ ($T_c = 0.158$ GeV). (b) \hat{q} as a function of the temperature T/T_c for an intermediate heavy quark momentum of $p_Q = 10$ GeV.

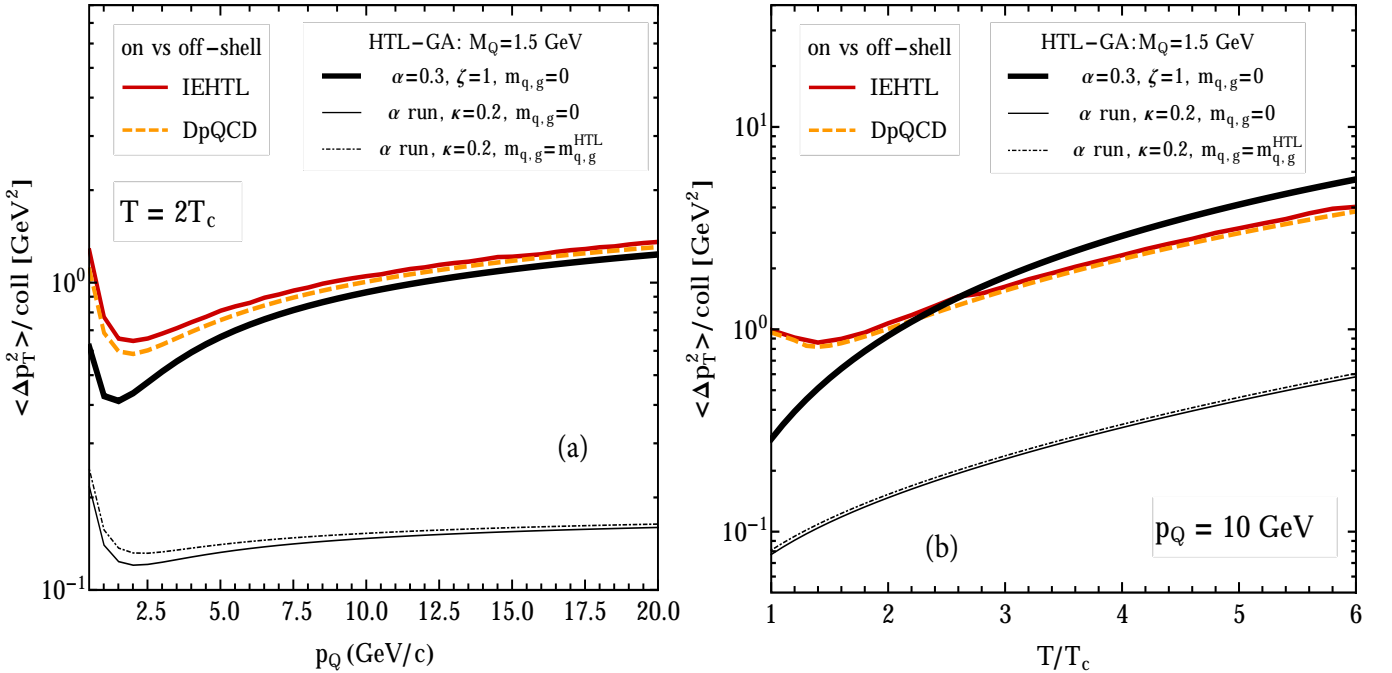


FIG. 12. (Color online) The transverse momentum transfer squared $\langle \Delta p_T^2 \rangle$ of c -quarks per collision in the plasma rest frame for the three different approaches: (a) as a function of the heavy quark momentum p_Q for $T = 2T_c$ ($T_c = 0.158$ GeV), (b) as a function of the temperature T/T_c for an intermediate heavy quark momentum of $p_Q = 10$ GeV.

and the trends observed in figs. 12 are explained.

We extend our model comparison for \hat{q} , as for η_D in Fig. 8, by including in Fig. 13 the standard pQCD result given by M&T

referring to Moore and Teaney (equation (B.32) with $\alpha = 0.3$ of [11]), HTL-B referring to Beraudo and al [50], with the two choices $\mu = 2\pi T$ and $\mu = \pi T$ (μ is a parameter in the coupling constant) and AdS/CFT to \hat{q} calculated in the framework of the anti de Sitter/conformal field $\mathcal{N} = 4$ SYM theory by Refs.[51–53]. HTL-GA (with $\alpha = 0.3$) and HTL-GA (with running α) refer to the two parameter sets of the HTL-GA model for constant and running coupling defined in [23]. For all calculations we have assumed the plasma temperature to be fixed to $T = 400$ MeV.

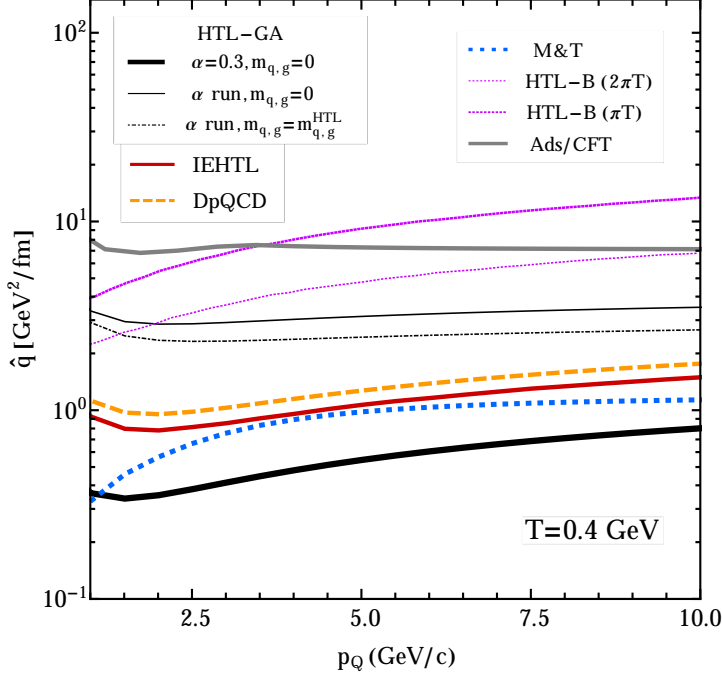


FIG. 13. (Color online) \hat{q} for c -quarks for different approaches as a function of the heavy quark momentum. The temperature of the scattering partners is $T = 400$ MeV. M&T refers to Moore and Teaney (equation (B.32) with $\alpha = 0.3$ of [11]), HTL-B referring to Beraudo and al. [50], with the two choices $\mu = 2\pi T$ and $\mu = \pi T$ (μ is a parameter in the coupling constant) and AdS/CFT to \hat{q} calculated in the framework of the anti de Sitter/conformal field $\mathcal{N} = 4$ SYM theory by Refs.[51–53]. HTL-GA (with $\alpha = 0.3$) and HTL-GA (with running α) refer to the two parameter sets of the HTL-GA model for constant and running coupling defined in [23].

The largest value for \hat{q} is given by AdS/CFT and HTL-B. The calculations in HTL-B are given in the spirit of the Hard Thermal Loop for the weak coupling limit of heavy quarks with the plasma partons. AdS/CFT predicts $\hat{q} = \frac{2}{v} \gamma^{1/2} \sqrt{\lambda} \pi T_{SYM}^3$, with $\gamma = 1/\sqrt{1-v^2}$ and $\lambda = g_{SYM}^2 N_c$; \hat{q} given by M&T in the framework of pQCD is slightly above the results from the DpQCD/IEHTL model.

VII. TRANSPORT CROSS SECTION AND CRITICAL ANALYSIS OF THE MODEL APPLICABILITY

In potential-scattering theory, the so called transport cross section is defined as the cross section weighted with $1 - \cos \theta$:

$$\sigma^{tr}(\mathbf{p}, T) = \int d\sigma (1 - \cos \theta) = \int \frac{d\sigma}{dt} (1 - \cos \theta(t)) dt, \quad (\text{VII.1})$$

where θ is the angle between the momentum of the outgoing and incoming particle measured in the lab frame. It is closely related to the transport coefficients [54, 55]. It has been introduced to have a measure for the momentum transfer in a single collision and gives a better possibility to compare different theories as the cross section itself because it weights the cross section by the average momentum transfer and suppresses small angle scattering which may have a large cross section but does not change much the momentum of the incoming particle. Therefore, the transport cross section is a more meaningful parameter to describe quark relaxation since QCD $2 \rightarrow 2$ interactions are usually forward-peaked, and so a large number of scatterings may map into a small changes of the momentum, only. For this purpose, we will first generalize the definition of the transport cross section to the case of scattering on finite mass particles and then present the results for the various models under study.

A. Relations between the transport cross section and the transport coefficients

In the case of a test particle propagating in a cell which contains finite mass particles distributed like f , different extensions of the definition (VII.1) are possible. Starting from the expression of the interaction rate Γ

$$\Gamma = \int f(s) v_{\text{rel}}(s) \sigma^{\text{tot}}(s) ds = \frac{v}{\ell}, \quad (\text{VII.2})$$

where ℓ is the mean free path, v is the relative velocity between the incident particle and the center of mass of the cell and v_{rel} is the relative velocity of this incident particle and one particles of the medium, one can define an effective total cross section as

$$\sigma_{\text{eff}}^{\text{tot}}(v; f) = \frac{\Gamma}{n v} = \frac{\int f(s) v_{\text{rel}}(s) \sigma^{\text{tot}}(s)}{v \int f(s) ds}, \quad (\text{VII.3})$$

where $n = \int d^3q / (2\pi)^3 f(q)$. From eq.(VII.3) it follows that the mean free path $\ell := \frac{1}{n \sigma_{\text{eff}}^{\text{tot}}}$ corresponds exactly to the interaction rate Γ . In the spirit of eq.(VII.3) one may define the transport cross section as,

$$\sigma_{\text{I}}^{\text{tr}}(v; f) = \frac{\int d^3q / (2\pi)^3 f(q) v_{\text{rel}}(q, p) \int \sigma (1 - \hat{p} \cdot \hat{p}')}{v \int d^3q / (2\pi)^3 f(q)}, \quad (\text{VII.4})$$

where \hat{p} (\hat{p}') is the direction of the initial (final) heavy quark momentum in the cell rest system. For a relativistic particle, $\|\mathbf{p}\| \approx \|\mathbf{p}'\|$ and at small scattering angles, $\cos \theta \approx 1 - \theta^2/2$, we can approximate $1 - \hat{p} \cdot \hat{p}' = 1 - \cos \theta \approx \frac{\sin^2 \theta}{2} \approx \frac{(\Delta p_T)^2}{2p^2}$. Then eq.(VII.4) becomes

$$\sigma_{\text{I}}^{\text{tr}}(v; f) = \frac{\int d^3q / (2\pi)^3 f(q) v_{\text{rel}}(q, p) \int \sigma (\Delta p_T)^2}{2np^2}. \quad (\text{VII.5})$$

The numerator of this expression is nothing but \hat{q} (VI.4), which measures the transverse momentum transfer squared per unit length. Hence, one obtains a first generalization of the transport cross section, which is directly proportional to \hat{q} :

$$\sigma_{\text{I}}^{\text{tr}}(v; f) = \frac{\hat{q}}{2np^2}. \quad (\text{VII.6})$$

to which one can associate a mean-free-path of diffusion given by $\ell^{\text{tr}} = \frac{1}{n \sigma_{\text{I}}^{\text{tr}}} = \frac{\hat{q}}{2p^2}$. As \hat{q} is given by $\langle \Delta p_T^2 \rangle / \ell$ with $\langle \Delta p_T^2 \rangle$ being the transverse momentum transfer squared in a single collision and $\ell = \frac{1}{n \sigma_{\text{tot}}}$, we find the relation

$$\ell^{\text{tr}} = \frac{2p^2}{\Delta p_T^2} \ell \gg \ell. \quad (\text{VII.7})$$

This mean free path of diffusion Eq. (VII.7) is the typical length after which the ultrarelativistic particle is deflected by a finite angle. It can thus be interpreted as a relaxation time of this angular evolution. For the purpose of describing heavy-quark transport, one can consider that an average heavy quark is undergoing a rather soft transverse momentum exchange of the order of $\langle \Delta p_T^2 \rangle$ every mean free path ℓ or, alternatively, a rather hard momentum exchange $\langle \Delta p_T^2 \rangle \times \frac{\ell^{\text{tr}}}{\ell}$ every ℓ^{tr} , both leading to the same \hat{q} value.

For the case of a potential scattering one has $\|\mathbf{p}\| = \|\mathbf{p}'\|$ and therefore an alternative generalization of the transport cross section is possible [54],

$$\sigma_{\text{II}}^{\text{tr}}(v; f) = \frac{\int d^3q / (2\pi)^3 f(q) v_{\text{rel}}(q, p) \int \sigma (1 - \frac{p'_L}{p})}{v \int d^3q / (2\pi)^3 f(q)}. \quad (\text{VII.8})$$

The numerator in (VII.8) is directly related to the drag coefficient (IV.4) and $\sigma_{\text{II}}^{\text{tr}}(v; f)$ becomes

$$\sigma_{\text{II}}^{\text{tr}}(v; f) = \frac{\hat{p}}{p} \cdot \frac{\mathbf{A}}{n v} = \frac{A}{p n v} = \frac{\eta_D}{n v}. \quad (\text{VII.9})$$

The relaxation time related to this transport coefficient is given by

$$\tau = \eta_D^{-1} = \frac{1}{n \sigma_{\text{II}}^{\text{tr}} v}, \quad (\text{VII.10})$$

Therefore, the transport cross section $\sigma_{\text{II}}^{\text{tr}}$ allows for the natural interpretation of a cross section that permits to evaluate the typical time after which a significant longitudinal momentum change has occurred. From eqs.(VII.6) and (VII.9), one concludes that the transport cross section might be related to the longitudinal momentum transfer, via the drag coefficient and to the transverse momentum transfer, via \hat{q} . The first interpretation is related to the slowing down of the heavy quark and the second to its transverse deflection. In pQCD, one has $A \propto \alpha^2 T^2 v$ and $\hat{q} \propto \alpha^2 T^3$ [11], so that

$$\sigma_{\text{I}}^{\text{tr}} \propto \frac{\alpha^2}{p^2} \ll \sigma_{\text{II}}^{\text{tr}} \propto \frac{\alpha^2}{pT} \ll \sigma \propto \frac{\alpha^2}{\mu^2}, \quad (\text{VII.11})$$

and one concludes that in pQCD most of the energy loss processes do not imply a large deflection. Let us insist that $\sigma_{\text{I}}^{\text{tr}} = \sigma_{\text{II}}^{\text{tr}}$ in potential scattering theory.

B. Transport cross sections in our models

We evaluated $\sigma_{\text{I}}^{\text{tr}}$ and $\sigma_{\text{II}}^{\text{tr}}$, as given by (VII.6) and (VII.9), for both the processes $q(g)c \rightarrow q(g)c$ for the models described in our study and report the values in figs. 14-(a) and 15-(a) as a function of the heavy quark momentum p_Q for $T = 2T_c$ and in figs. 14-(b) and 15-(b) as a function of the temperature for $p_Q = 10$ GeV. These figures show that the large difference seen in the total cross sections between the HTL-GA and DpQCD/IEHTL models is reduced significantly for the transport cross section. Indeed, whereas the total cross section is dominated by an infrared divergence, the transport cross section weights the square of the matrix element with $|t|$. As for the previous transport coefficients (drag and \hat{q}), the increase of the parton mass leads to a decrease of $\sigma_{\text{II}}^{\text{tr}}$ and to an increase of $\sigma_{\text{I}}^{\text{tr}}$. Figs. 14-(b) and 15-(b) show that for temperatures near T_c , the transport cross section is larger in DpQCD/IEHTL compared to the HTL-GA model. Due to the enhancement of the coupling constant, the DpQCD/IEHTL model gives the largest value of the transport cross sections for temperatures smaller than $2T_c$. For $T > 2T_c$, the HTL-GA transport cross section is the largest one for all heavy quark momenta but the gap is smaller as compared to the total cross section (cf. Ref.[28]). Figs. 14-(a), (b) and 15-(a), (b) show also that the off-shell effects are almost washed out for the transport cross section as in the case of the total cross section.

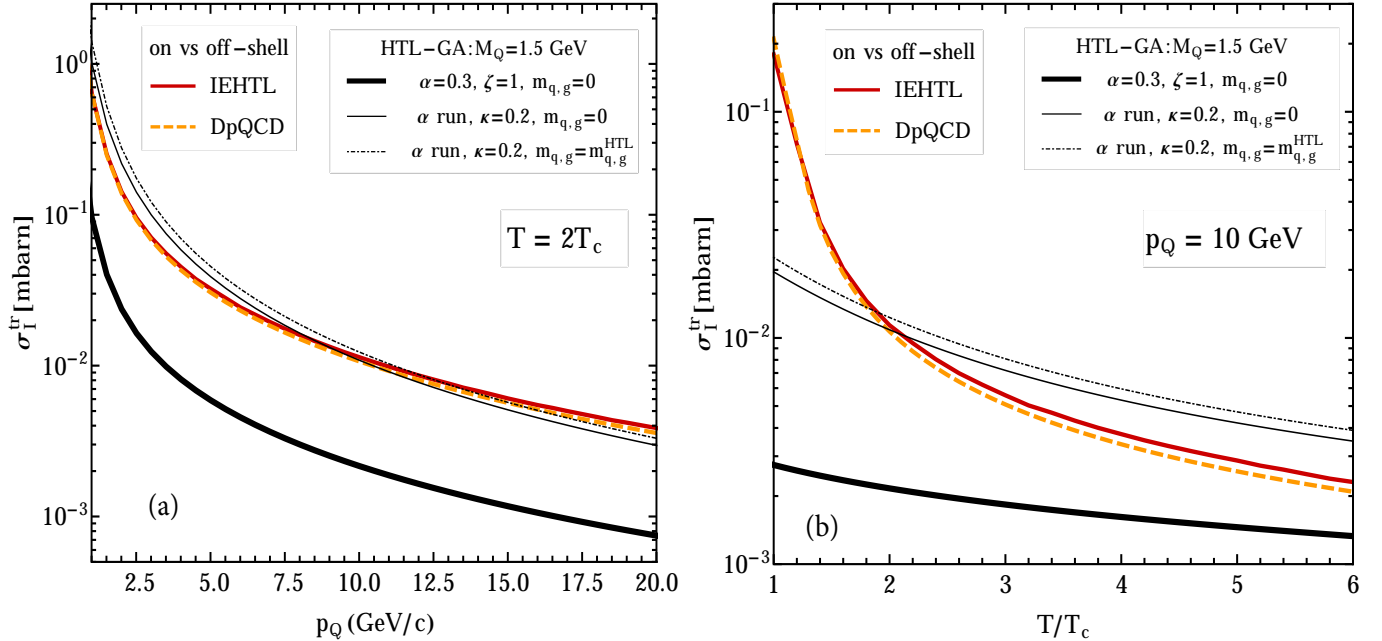


FIG. 14. (Color online) The total transport cross section $\sigma_{\text{I}}^{\text{tr}}$ (VII.6) for the $q(g)c \rightarrow q(g)c$ processes for the three different approaches as a function of the heavy quark momentum p_Q for $T = 2T_c$ (left) and as a function of the temperature T/T_c ($T_c = 0.158$ GeV) for an intermediate heavy quark momentum, $p_Q = 10$ GeV (right).

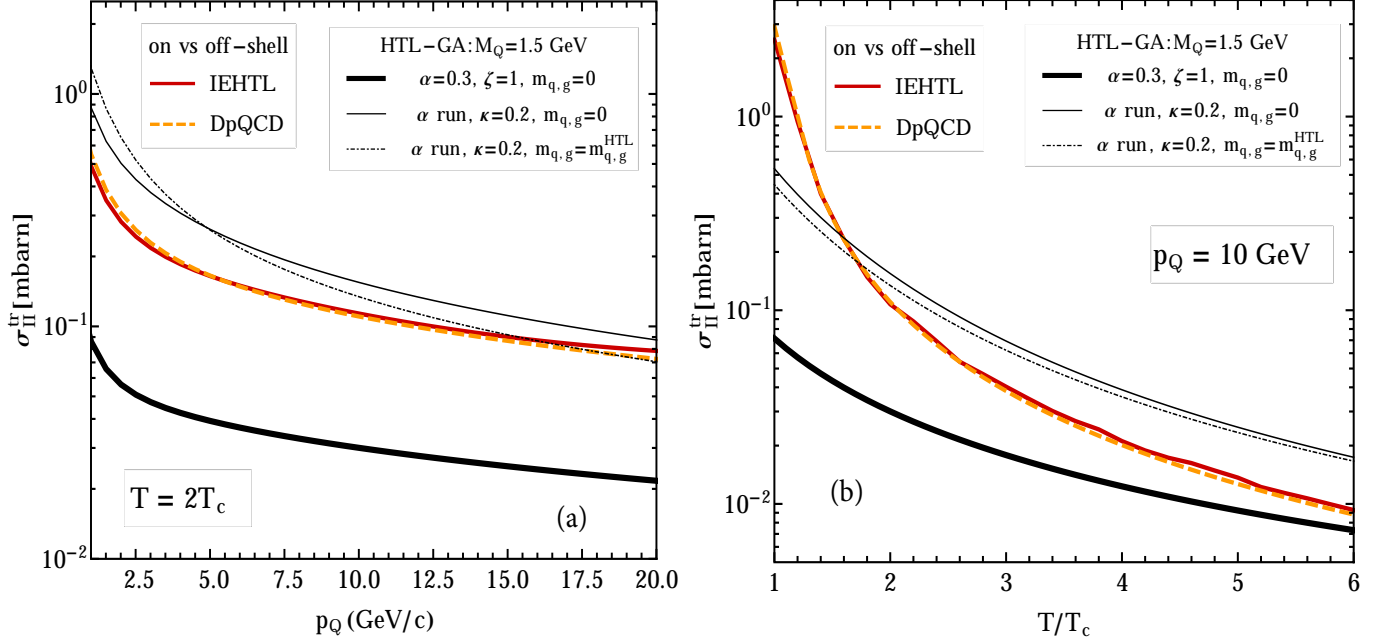


FIG. 15. (Color online) The total transport cross section σ_{II}^{tr} (VII.9) for the $q(g)c \rightarrow q(g)$ processes for the three different approaches as a function of the heavy quark momentum p_Q for $T = 2T_c$ (left) and as a function of the temperature T/T_c ($T_c = 0.158$ GeV) for an intermediate heavy quark momentum, $p_Q = 10$ GeV (right).

C. Microscopic interpretation of σ^{tr} and applicability of Boltzmann transport

In a microscopic approach based on the diffusion of a heavy quark with a particle of effective mass $m_{q/g}^{\text{eff}} = \sqrt{m_{q/g}^2 + T^2}$ at rest, one can show that the cross section eq.(VII.6) for $p \gg m = \{m_q, m_g, M_Q, T\}$ is given by

$$\sigma_I^{\text{tr}} \sim \frac{1}{p^2} \int_{-|t|_{\text{max}}}^0 |t| \frac{d\sigma}{dt} dt, \quad (\text{VII.12})$$

whereas σ_{II}^{tr} (VII.9) can be expressed by

$$\sigma_{II}^{\text{tr}} \sim \frac{1}{2m_{q/g}^{\text{eff}} p} \int_{-|t|_{\text{max}}}^0 |t| \frac{d\sigma}{dt} dt. \quad (\text{VII.13})$$

Both transport cross sections are related by

$$\sigma_I^{\text{tr}} \sim \frac{2m_{q/g}^{\text{eff}}}{p} \sigma_{II}^{\text{tr}}. \quad (\text{VII.14})$$

Therefore it follows:

$$\sigma_I^{\text{tr}} \ll \sigma_{II}^{\text{tr}} \ll \sigma^{\text{tot}}, \quad (\text{VII.15})$$

and the following relation holds between \hat{q} and A

$$\hat{q} \sim 2m_{q/g}^{\text{eff}} A. \quad (\text{VII.16})$$

From eqs.(VII.12) and (VII.13), we conclude that the differences in the transport cross sections between the HTL-GA and DpQCD/IEHTL are related to the quantity $\langle \sigma |t| \rangle = \int \frac{d\sigma}{dt} |t| dt$. $\langle \sigma |t| \rangle$ for the elastic qQ scattering is plotted in figure 7-(b) and compared to the total cross section σ^{qQ} presented in fig.7-(a) following the models HTL-GA with α running and DpQCD. Whereas σ^{qQ} is much larger in HTL-GA, the difference between HTL-GA and DpQCD for $\langle \sigma |t| \rangle$ is reduced, which explains the profiles seen in figs. 14-(a), (b) and 15-(a), (b).

To check the relation between σ_I^{tr} and σ_{II}^{tr} (VII.14), we plot the ratio $\sigma_I^{\text{tr}}/\sigma_{II}^{\text{tr}}$ as a function of the heavy quark momentum p_Q in figure 16-(a) and as a function of the temperature in fig.16-(b). From these figures, we see clearly that $\sigma_I^{\text{tr}}/\sigma_{II}^{\text{tr}} \propto p_Q^{-1} = p^{-1}$ for a given temperature and $\sigma_I^{\text{tr}}/\sigma_{II}^{\text{tr}} \propto T$ for a given heavy quark momentum and therefore the relation (VII.14) is verified as $m_{q/g}^{\text{eff}} \propto T$. Furthermore, we can approximate from eqs.(IV.22) and (VI.11) the ratio $\sigma_I^{\text{tr}}/\sigma_{II}^{\text{tr}}$ for the interaction of a heavy quark with a massive light quark to

$$\sigma_{I,qQ}^{\text{tr}}/\sigma_{II,qQ}^{\text{tr}} = \frac{\hat{q}}{2EA} \propto \frac{m_q}{2E}. \quad (\text{VII.17})$$

Since m_q and m_g are proportional to the temperature and in addition $m_q^{DQPM} > m_q^{HTL}$, the relation in eq.(VII.17) is well reproduced in fig. 16-(b) including the mass hierarchy between the models HTL-GA with finite $m_{q,g}$ and DpQCD/IEHTL.

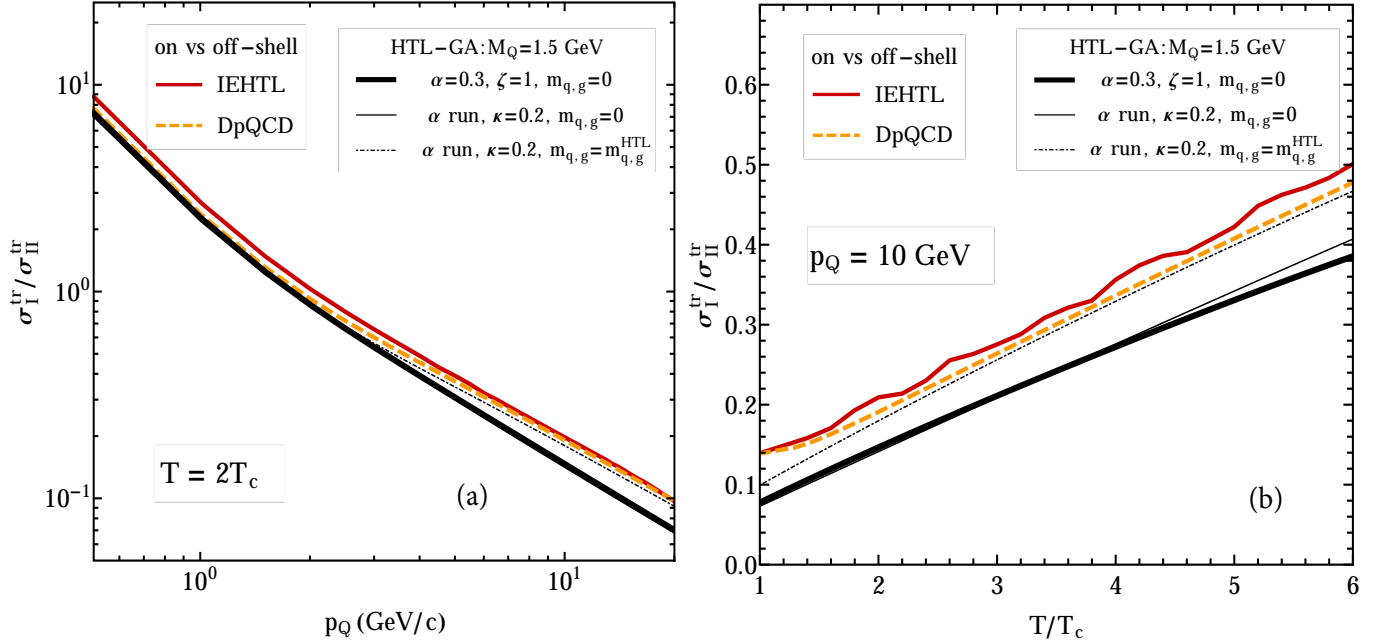


FIG. 16. (Color online) The ratio $\sigma_I^{\text{tr}}/\sigma_{II}^{\text{tr}}$ as a function of the heavy-quark momentum p_Q for $T = 2T_c$ (left) and as a function of the temperature for $p_Q = 10 \text{ GeV}$ (right). We note that $\sigma_I^{\text{tr}}/\sigma_{II}^{\text{tr}} = \sigma_{I,qQ}^{\text{tr}}/\sigma_{II,qQ}^{\text{tr}} + \sigma_{I,gQ}^{\text{tr}}/\sigma_{II,gQ}^{\text{tr}}$.

Present transport approaches describing the propagation of heavy flavor particles inside the QGP rely either on the phenomenological Langevin dynamics or on the Boltzmann equation. This equation is legitimate under the assumptions of diluteness and of molecular chaos [56], achieved provided the mean free path ℓ is much larger than the interaction range $d \simeq \mu^{-1}$. An equivalent criterion is to require that the relaxation time $\tau = \langle R \rangle^{-1}$ (III.6) should be larger than the collision time τ_{int} for a $Qq \rightarrow Qq$ or $Qg \rightarrow Qg$ process, with $\tau_{\text{int}} \simeq (\mu \langle v_{\text{rel}} \rangle)^{-1} \approx \mu^{-1}$.

Comparing fig. 4 (left) with fig. 2 (right), one can check that this criteria is indeed satisfied for all values of T in the case of the DpQCD/IEHTL models, while it is never satisfied for the HTL-GA model with α running. Although this could cast doubt upon the applicability of the Boltzmann transport in this case, one has to remind that most of the collisions in the GA model do not lead to large momentum transfer (as seen from fig. 6) and are thus inefficient for the deceleration of heavy quarks. One therefore obtains a more suitable criteria by considering, instead of the relaxation time (III.6), the one associated with the transport cross section σ_{II}^{tr} , as defined in Eq. (VII.10). For $p \approx 0$, one obtains $\eta_D/\mu \approx 0.3$ (see Fig. 8) in the HTL-GA model with α running, and this ratio even decreases $\propto p^{-1}$ at finite p . This implies that the time interval between 2 subsequent collisions relevant for the momentum transfers is indeed larger than the interaction time, which legitimates the use of the Boltzmann equation for this model as well.

VIII. SUMMARY

We have studied the transport coefficients for three different effective theories (or models) which are based on cross sections calculated in the Born approximation. The latter cross sections have perturbative or non-perturbative elements of QCD:

- a) the HTL-GA model which employs a running coupling and an effective infrared regulator whose value is adjusted to hard thermal loop calculations [23]. In this model quarks and gluons have either no mass or a mass which depends linearly on the temperature.
- b) the DpQCD approach in which on-shell quarks and gluons have a thermal mass which is adjusted to reproduce lattice gauge calculation in equilibrium at finite temperature T . This model employs a running coupling (in T/T_c) and is in accord with lattice QCD correlators for the shear and bulk viscosities for finite T [57].
- c) the IEHTL which takes fully into account the off-shell character of the quarks and gluons and contains the DpQCD masses as pole masses.

For each of these models we have calculated the interaction rates, the c -quark drag and diffusion coefficient, the longitudinal and transverse momentum broadening and the transport cross section.

Our study has demonstrated that even if the influence of the finite width of the quasi-particles on heavy quark scattering is negligible for the off-shell heavy quark Q scattering cross sections [28], a noticeable effect is seen in the off-shell transport coefficients (IEHTL model) compared to their on-shell counterparts (DpQCD model). This is essentially due to the reduced kinematical threshold in the off-shell cross sections and mass effects. The finite width of the IEHTL model lowers the interaction rate and therefore as well the drag and diffusion coefficients. Also \hat{q} becomes smaller but all these differences are on the level of 10-20%. For temperatures ($T > 3T_c$) the drift coefficient in the HTL-GA model with a fixed coupling α and zero mass partons and that of DpQCD are not very different. This is also true for the energy loss dE/dx . For higher temperatures the HTL-GA model shows a larger stopping because the increasing mass in the DpQCD approach (with temperature) lowers the interaction rate substantially without leading to a much higher stopping in an individual collision of a heavy quark with the plasma particles.

Our survey has provided a comprehensive comparison between perturbative and non-perturbative QCD based models on the determination of the heavy quark transport coefficients. Furthermore, the phenomenological consequences of using HTL-GA and DpQCD/IEHTL cross sections (as determined in Ref.[28]) on the heavy quark collective transport have been presented in detail. A significant differences between HTL-GA and DpQCD/IEHTL models has been pointed out for the different heavy-quark transport characteristics. However, the comparisons have to be carried out with some notes of caution. Indeed, even if the HTL-GA for a running coupling gives the largest heavy quark drag coefficient and interaction rates compared to the other models, the heavy quark longitudinal and transverse momentum fluctuations are smaller.

The final goal of our investigation is to figure out the main differences between two models based on perturbative or non-perturbative effective QCD models on one side and two concepts for the heavy quark diffusion in a medium with many massless light quarks and gluons or a few massive/off-shell q and g , respectively. Our finding is that explicit transport calculations in comparison to experimental data are needed to figure out the appropriate scenario as a function of collision centrality and bombarding energy, since the microscopic ingredients (fixed or running couplings in momentum or temperature) and the QGP background description (massless or massive degrees of freedom) are strongly coupled and specific to each model.

The heavy quark scattering cross sections obtained in Ref.[28] and the heavy quark transport properties illustrated in this study will form the basis of a consistent calculation of the heavy quark propagation and dynamics in heavy-ion collisions at SPS, RHIC and LHC energies by implementing the partonic processes into the transport approach of the PHSD collaboration to study heavy-quark dynamics at SPS, RHIC and LHC energies as a function of centrality. These future studies will also address the momentum correlations of $c\bar{c}$ pairs (or $D\bar{D}$ pairs) as a function of rapidity and transverse momentum.

ACKNOWLEDGMENT

H. Berrehrah thanks R. Marty for fruitful discussions and his continuous interest. He also acknowledges the ‘‘HIC for FAIR’’ framework of the ‘‘LOEWE’’ program and the ‘‘Together project of the region Pays de la Loire’’ for support of this work. The computational resources were provided by the LOEWE-CSC.

APPENDIX

Appendix A: Elastic interaction rate for off-shell partons

The covariant off-shell rate $\mathcal{R}^{\text{off}} = \frac{dN_{\text{coll}}^{\text{off}}}{d\tau}$ is given by

$$\mathcal{R}^{\text{off}}(T) = \frac{1}{(2\pi)^9} \int d\omega \frac{E_p}{M_Q} \rho_p(p) \Theta(\omega_p) \int d^4q f(q) \rho_q(q) \Theta(\omega_q) r^{\text{off}}(s, T),$$

$$r^{\text{off}}(s, T) := \int d^4q' \int d^4p' \rho_{p'}(p') \rho_{q'}(q') \Theta(\omega_{p'}) \Theta(\omega_{q'}) \delta^{(4)}(P_{in} - P_{fin}) \frac{1}{g_p g_Q} \sum_{k,l} |\mathcal{M}_{2,2}^{\text{off}}(p, q; i, j | p', q'; k, l)|^2. \quad (\text{A.1})$$

We proceed following the same procedure as for the on-shell case. Nevertheless, the derivation of the explicit expression for $\mathcal{R}^{\text{off}}(T)$ and $r^{\text{off}}(s, T)$ depends on the choice of the parton spectral function which we will consider. We will give the expressions for both, the Lorentzian- ω form and the Breit-Wigner- m for of the parton spectral functions.

- For the Lorentzian- ω form of the spectral function:

In a complete off-shell picture $\mathcal{R}^{\text{off}}(T)$ depends only on the medium temperature since we convolute with the mass and momentum spectral functions. r^{off} is explicitly given by

$$\begin{aligned} r^{\text{off}}(s, T) &:= \int E_{q'} d\omega_{q'} \rho_{q'}^L(\omega_{q'}) \int E_{p'} d\omega_{p'} \rho_{p'}^L(\omega_{p'}) \int \frac{d^3 q'}{E_{q'}} \int \frac{d^3 p'}{E_{p'}} \delta^{(4)}(P_{in} - P_{fin}) \frac{1}{g_p g_Q} \sum_{k,l} |\mathcal{M}_{2,2}^{\text{off}}(p, q; i, j | p', q'; k, l)|^2(s, t). \\ &= \int E_{q'} d\omega_{q'} \rho_{q'}^L(\omega_{q'}) \int E_{p'} d\omega_{p'} \rho_{p'}^L(\omega_{p'}) \frac{\pi}{\sqrt{s} p_{cm}(s)} \int_{t_{min}}^{t_{max}} \frac{1}{g_p g_Q} \sum_{k,l} |\mathcal{M}_{2,2}^{\text{off}}(p, q; i, j | p', q'; k, l)|^2(s, t) dt, \end{aligned} \quad (\text{A.2})$$

where t_{min} and t_{max} are given by:

$$\begin{aligned} t_{min}^{max} &= -\frac{s}{2} \left(1 - (\beta_1 + \beta_2 + \beta_3 + \beta_4) + (\beta_1 - \beta_2)(\beta_3 - \beta_4) \pm \sqrt{(1 - \beta_1 - \beta_2)^2 - 4\beta_1\beta_2} \sqrt{(1 - \beta_3 - \beta_4)^2 - 4\beta_3\beta_4} \right) \\ \text{with: } \beta_1 &= (m_q^i)^2/s, \beta_2 = (M_Q^i)^2/s, \beta_3 = (m_q^f)^2/s, \beta_4 = (M_Q^f)^2/s. \end{aligned} \quad (\text{A.3})$$

The remaining integral in (A.1) is evaluated in the rest frame of the heavy quark and can be calculated in a similar way as for the on-shell case with a special care on the convolution with the parton spectral functions.

- For the Breit-Wigner- m form of the spectral function:

Considering the Breit-Wigner- m for the spectral functions, valid in the non-relativistic limit, the expression for $Tr_{(i)}^{\text{on}} = \sum_i \int \frac{d^3 p_i}{(2\pi)^3} \frac{1}{2E_{p_i}}$ becomes in the off-shell case $Tr_{(i)}^{\text{off}} = \sum_i \int \frac{dm_i}{(2\pi)} \frac{m_i}{\sqrt{m_i^2 + \mathbf{p}_i^2}} \rho_i^{BW}(m_i) \int \frac{d^3 p}{(2\pi)^3}$. Then $\mathcal{R}^{\text{off}}(T)$ and $r^{\text{off}}(s, T)$ are simply obtained from the on-shell case where we should convolute with the different parton spectral functions in mass. Therefore, for a Breit-Wigner- m parton spectral function the expressions in (A.1) become

$$\begin{aligned} \mathcal{R}^{\text{off}}(T) &= \frac{1}{(2\pi)^9} \int dm_p \rho_p^{BW}(m_p) \int m_q dm_q \rho_q^{BW}(m_q) \int \frac{d^3 q}{E_q} f(\mathbf{q}) r^{\text{off}}(s, T), \\ r^{\text{off}}(s, T) &:= \int m_{q'} dm_{q'} \rho_{q'}^{BW}(m_{q'}) \int m_{p'} dm_{p'} \rho_{p'}^{BW}(m_{p'}) \int \frac{d^3 q'}{E_{q'}} \int \frac{d^3 p'}{E_{p'}} \delta^{(4)}(P_{in} - P_{fin}) \frac{1}{g_p g_Q} \sum_{k,l} |\mathcal{M}_{2,2}^{\text{off}}(p, q; i, j | p', q'; k, l)|^2(s, t). \\ &= \int m_{q'} dm_{q'} \rho_{q'}^{BW}(m_{q'}) \int m_{p'} dm_{p'} \rho_{p'}^{BW}(m_{p'}) \frac{\pi}{\sqrt{s} p_{cm}(s)} \int_{t_{min}}^{t_{max}} \frac{1}{g_p g_Q} \sum_{k,l} |\mathcal{M}_{2,2}^{\text{off}}(p, q; i, j | p', q'; k, l)|^2(s, t) dt. \end{aligned} \quad (\text{A.4})$$

By direct analogy to the on-shell case, $R^{\text{off}}(\mathbf{p})$ becomes

$$R^{\text{off}}(\mathbf{p}) = \Pi_{i \in p, q, p', q'} \int m_i dm_i \rho_i^{BW}(m_i) \frac{m_p}{8(2\pi)^3 E_p} \int \frac{q^3 m_0^{\text{off}}(s) f_0(\frac{p}{M_Q}; q)}{s E_q} dq, \quad (\text{A.5})$$

where

$$\begin{aligned} m_0^{\text{off}}(s) &= \int_{-1}^{+1} d\cos\theta \sum |\mathcal{M}_{2,2}^{\text{off}}(p, q; i, j | p', q'; k, l)|^2(s, t) = \frac{1}{2p_{cm}^2(s)} \int_{t_{min}}^{t_{max}} \sum |\mathcal{M}_{2,2}^{\text{off}}(p, q; i, j | p', q'; k, l)|^2(s, t) dt, \\ f_0\left(\frac{p}{M_Q}; q\right) &= \frac{1}{2} \int \frac{d\cos\theta_r}{\exp(u^0 E_q - q u \cos\theta_r) \pm 1}, \end{aligned} \quad (\text{A.6})$$

and $\sum |\mathcal{M}_{2,2}^{\text{off}}(p, q; i, j | p', q'; k, l)|^2(s, t)$ the off-shell transition amplitude defined in IEHTL approach, Ref.[28].

Appendix B: Drag coefficient for off-shell partons

Similarly to the transition from the on-shell to the off-shell limits for the study of the interaction rates, one deduces the corresponding expression for A_i^{off} , the drag coefficient for the off-shell case,

$$A_i^{\text{off}}(T) = \frac{1}{(2\pi)^9} \int d\omega \int d^4q f(\mathbf{q}) \int d^4q' \int d^4p' \rho_p(p) \rho_q(q) \rho_{p'}(p') \rho_{q'}(q') \Theta(\omega_p) \Theta(\omega_q) \Theta(\omega_{p'}) \Theta(\omega_{q'}) \\ \times (p - p')_i \delta^{(4)}(P_{in} - P_{fin}) \frac{1}{g_p g_Q} \sum_{k,l} |\mathcal{M}_{2,2}^{\text{off}}(p, q; i, j | p', q'; k, l)|^2(s, t), \quad (\text{B.1})$$

where, by writing $\frac{1}{2E_p} = \int_0^\infty \frac{d\omega}{2\pi} 2\pi \delta(\omega^2 - E_p^2)$, the transition from the on-shell case to the off-shell case is characterized by $\frac{1}{2E_p} \rightarrow \int_0^\infty \frac{d\omega}{2\pi} \rho_p(\omega, \mathbf{p}) = \int \frac{d\omega}{2\pi} \rho_p(\omega, \mathbf{p}) \theta(\omega)$. Therefore, $\mathcal{A}^{\text{off}} = \frac{dp_i^{\text{off}}}{d\tau}$ becomes

$$\mathcal{A}_{\text{off}}^\mu(T) = -\frac{1}{(2\pi)^9} \int d\omega \frac{E_p}{M_Q} \rho_p(p) \Theta(\omega_p) \int d^4q f(\mathbf{q}) \rho_q(q) \Theta(\omega_q) a_{\text{off}}^\mu(\mathbf{p}), \quad (\text{B.2}) \\ a_{\text{off}}^\mu(\mathbf{p}) := \int d^4q' \int d^4p' \rho_{p'}(p') \rho_{q'}(q') \Theta(\omega_{p'}) \Theta(\omega_{q'}) (q - q')^\mu \delta^{(4)}(P_{in} - P_{fin}) \frac{1}{g_p g_Q} \sum_{k,l} |\mathcal{M}_{2,2}^{\text{off}}(p, q; i, j | p', q'; k, l)|^2(s, t).$$

We then proceed following the same procedure as for the on-shell case. Nevertheless, the derivation of the explicit expression for $\mathcal{A}_{\text{off}}^\mu(T)$ and $a_{\text{off}}^\mu(\mathbf{p})$ depends on the choice of the parton spectral function. If the Lorentzian- ω form of the parton spectral function is considered then we should derive a new expression for $\mathcal{A}_{\text{off}}^\mu(T)$ and $a_{\text{off}}^\mu(\mathbf{p})$ since the running energy involves a running of the different parton momenta. On the other hand, if we consider the Breit-Wigner- m form of the spectral functions valid in the non-relativistic limit, then $\mathcal{A}_{\text{off}}^\mu(T)$ and $a_{\text{off}}^\mu(\mathbf{p})$ are simply obtained from the on-shell case by convoluting this expression with the different parton spectral functions and the transition from the on- to off-shell case can be factorized. Therefore, for a Breit-Wigner- m parton spectral function the expressions (B.2) become

$$\mathcal{A}_{\text{off}}^\mu(T) = -\frac{1}{(2\pi)^9} \int dm_p \rho_p^{\text{BW}}(m_p) \int m_q dm_q \rho_q^{\text{BW}}(m_q) \int \frac{d^3q}{E_q} f(\mathbf{q}) a_{\text{off}}^\mu(\mathbf{p}), \quad (\text{B.3}) \\ a_{\text{off}}^\mu(\mathbf{p}) := \int m_q dm_q \rho_q^{\text{BW}}(m_q) \int m_{p'} dm_{p'} \rho_{p'}^{\text{BW}}(m_{p'}) \int \frac{d^3q'}{E_{q'}} \int \frac{d^3p'}{E_{p'}} (q - q')^\mu \delta^{(4)}(P_{in} - P_{fin}) \frac{1}{g_p g_Q} \sum_{k,l} |\mathcal{M}_{2,2}^{\text{off}}(p, q; i, j | p', q'; k, l)|^2(s, t).$$

In the cm frame, we find for a_{cm}^{off}

$$a_{cm}^{\text{off}} = \int m_{q'} dm_{q'} \rho_{q'}^{\text{BW}}(m_{q'}) \int m_{p'} dm_{p'} \rho_{p'}^{\text{BW}}(m_{p'}) \frac{4\pi p_{cm}^2(s)}{\sqrt{s}} m_1^{\text{off}}(s) \times \hat{\mathbf{q}}_{cm}, \\ \text{with: } m_1^{\text{off}}(s) := \frac{1}{4p_Q^i p_Q^f} \int_{t_{min}}^{t_{max}} \sum |\mathcal{M}_{2,2}^{\text{off}}(p, q; i, j | p', q'; k, l)|^2(s, t) \left[1 - \frac{t - (M_Q^i)^2 + (M_Q^f)^2 - 2E_Q^i E_Q^f}{2p_Q^i p_Q^f} \right] dt, \quad (\text{B.4})$$

where p_Q^i (M_Q^i) is the initial heavy quark momentum (mass) and p_Q^f (M_Q^f) is the final heavy quark momentum (mass). In the heavy quark rest frame a_{rest}^{off} is given by

$$a_{rest}^{\text{off}} = \int m_{q'} dm_{q'} \rho_{q'}^{\text{BW}}(m_{q'}) \int m_{p'} dm_{p'} \rho_{p'}^{\text{BW}}(m_{p'}) \frac{4\pi p_{cm}^2(s)}{s} m_1^{\text{off}}(s) \left((E_{q_{rest}} + m_Q) \hat{\mathbf{q}}_{cm} \right), \quad (\text{B.5})$$

which leads to the following expressions of $A_{rest}^{0,\text{off}}$ and $A_{rest}^{v,\text{off}}$

$$A_{rest}^{0,\text{off}} = \frac{4}{(2\pi)^7} \Pi_{i \in p, q, p', q'} \int m_p m_i dm_i \rho_i^{\text{WB}}(m_i) \int_0^\infty \frac{q^5 m_1(s) f_0(q)}{s^2 E_q} dq, \quad (\text{B.6}) \\ A_{rest}^{v,\text{off}} = \frac{4}{(2\pi)^7} \Pi_{i \in p, q, p', q'} \int m_p m_i dm_i \rho_i^{\text{WB}}(m_i) \int_0^\infty \frac{q^4 (M_Q + E_q) m_1(s) f_1(q)}{s^2 E_q} dq.$$

Finally the drag coefficient for the off-shell partons in the heat bath rest frame is given by

$$\mathbf{A}_{\text{heat bath}}^{\text{off}} = \left(A_{\text{rest}}^{\text{v,off}} - \tilde{A}_{\text{rest}}^{0,\text{off}} \right) \hat{\mathbf{p}}, \quad (\text{B.7})$$

where $\tilde{A}_{\text{rest}}^{0,\text{off}}$ and $\tilde{A}_{\text{rest}}^{\text{v,off}}$ are defined by

$$\begin{aligned} \tilde{A}_{\text{rest}}^{0,\text{off}} &= \frac{4}{(2\pi)^7} \Pi_{i \in p, q, p', q'} \int \frac{p}{E_p} \frac{m_p}{m_i} dm_i \rho_p^{\text{WB}}(m_i) \int_0^\infty \frac{q^5 m_1(s) f_0(q)}{s^2 E_q} dq, \\ \tilde{A}_{\text{rest}}^{\text{v,off}} &= \frac{4}{(2\pi)^7} \Pi_{i \in p, q, p', q'} \int \frac{p}{E_p} \frac{m_p}{m_i} dm_i \rho_p^{\text{WB}}(m_i) \int_0^\infty \frac{q^4 (M_Q + E_q) m_1(s) f_1(q)}{s^2 E_q} dq. \end{aligned} \quad (\text{B.8})$$

Appendix C: Dynamical collisional energy loss for off-shell partons

The collisional energy loss for on-shell partons (I.1) can be easily extended to the off-shell case. The covariant $\frac{dE^{\text{off}}}{d\tau}$ is given by

$$\begin{aligned} \frac{dE^{\text{off}}}{d\tau}(T) &= \frac{1}{(2\pi)^9} \int d\omega \frac{E_p}{M_Q} \int d^4 q f(\mathbf{q}) \int d^4 q' \int d^4 p' \rho_p(p) \rho_q(q) \rho_{p'}(p') \rho_{q'}(q') \Theta(\omega_p) \Theta(\omega_q) \Theta(\omega_{p'}) \Theta(\omega_{q'}) \\ &\quad \times (E - E') \delta^{(4)}(P_{\text{in}} - P_{\text{fin}}) \frac{1}{g_p g_Q} \sum_{k,l} |\mathcal{M}_{2,2}^{\text{off}}(p, q; i, j | p', q'; k, l)|^2(s, t), \end{aligned} \quad (\text{C.1})$$

therefore, $\frac{dE^{\text{off}}}{d\tau}$ becomes

$$\begin{aligned} \frac{dE^{\text{off}}}{d\tau}(T) &= -\frac{1}{(2\pi)^9} \int d\omega \frac{E_p}{M_Q} \rho_p(p) \Theta(\omega_p) \int d^4 q f(\mathbf{q}) \rho_q(q) \Theta(\omega_q) e^{\text{off}}(\mathbf{p}), \\ e^{\text{off}}(\mathbf{p}) &:= \int d^4 q' \int d^4 p' \rho_{p'}(p') \rho_{q'}(q') \Theta(\omega_{p'}) \Theta(\omega_{q'}) (E - E') \delta^{(4)}(P_{\text{in}} - P_{\text{fin}}) \frac{1}{g_p g_Q} \sum_{k,l} |\mathcal{M}_{2,2}^{\text{off}}(p, q; i, j | p', q'; k, l)|^2(s, t). \end{aligned} \quad (\text{C.2})$$

As for the drag coefficient the explicit expressions of $\frac{dE^{\text{off}}}{d\tau}$ and $e^{\text{off}}(\mathbf{p})$ depend on the choice of the parton spectral function. For this study we consider the Breit-Wigner- m form of the spectral functions, then $\frac{dE^{\text{off}}}{d\tau}$ and $e^{\text{off}}(\mathbf{p})$ are simply obtained from the on-shell case by convoluting these expressions with the different parton spectral functions and the transition from the on- to off-shell case can be factorized again. Using Breit-Wigner- m spectral functions (C.2) becomes

$$\begin{aligned} \frac{dE^{\text{off}}}{d\tau}(T) &= -\frac{1}{(2\pi)^9} \int dm_p \rho_p^{\text{BW}}(m_p) \int m_q dm_q \rho_q^{\text{BW}}(m_q) \int \frac{d^3 q}{E_q} f(\mathbf{q}) e^{\text{off}}(\mathbf{p}), \\ e^{\text{off}}(\mathbf{p}) &:= \int m_{q'} dm_{q'} \rho_{q'}^{\text{BW}}(m_{q'}) \int m_{p'} dm_{p'} \rho_{p'}^{\text{BW}}(m_{p'}) \int \frac{d^3 q'}{E_{q'}} \int \frac{d^3 p'}{E_{p'}} (E - E') \delta^{(4)}(P_{\text{in}} - P_{\text{fin}}) \frac{1}{g_p g_Q} \sum_{k,l} |\mathcal{M}_{2,2}^{\text{off}}(p, q; i, j | p', q'; k, l)|^2(s, t). \end{aligned} \quad (\text{C.3})$$

Proceeding as for the drag coefficient for the off-shell partons, $\frac{dE^{\text{off}}}{dt}(T)$ is given by

$$\frac{dE^{\text{off}}}{dt}(T) = A_{\text{rest}}^{0,\text{off}} - \tilde{A}_{\text{rest}}^{\text{v,off}}, \quad (\text{C.4})$$

where $A_{\text{rest}}^{0,\text{off}}$ and $\tilde{A}_{\text{rest}}^{\text{v,off}}$ are defined in (B.6) and (B.8).

Appendix D: \hat{q} for on-shell partons

For a massive on-shell parton, B_T , and then \hat{q} is obtained following the same procedure as for the evaluation of the drag coefficient. Using (VI.1) and (VI.3), one finds that b^{ij} , written in the c.m frame by

$$b_{cm}^{ij}(\mathbf{p}) = \frac{p_{cm}}{\sqrt{s}} \int \frac{d^3 q'}{2E_{q'}} \int \frac{d^3 p'}{2E_{p'}} \frac{(q - q')^i (q - q')^j}{2} \delta^{(4)}(P_{in} - P_{fin}) \frac{1}{g_p g_Q} \sum_{k,l} |\mathcal{M}_{2,2}^{\text{on}}(p, q; i, j | p', q'; k, l)|^2(s, t) \quad (\text{D.1})$$

can be decomposed in its transverse $b_{cm,T}$ and longitudinal $b_{cm,L}$ components

$$b_{cm}^{ij}(\mathbf{p}) = b_{cm,T}(I - |\hat{q}_{cm} \rangle \langle \hat{q}_{cm}|) + b_{cm,L}|\hat{q}_{cm} \rangle \langle \hat{q}_{cm}|, \quad (\text{D.2})$$

with

$$\begin{aligned} b_{T,cm}(\mathbf{p}) &= \frac{p_{cm}}{2\sqrt{s}} \int \frac{d^3 q'}{2E_{q'}} \int \frac{d^3 p'}{2E_{p'}} \left(\frac{\|\mathbf{q} - \mathbf{q}'\|^2}{2} - \frac{((\mathbf{q} - \mathbf{q}') \cdot \hat{q})^2}{2} \right) \delta^{(4)}(P_{in} - P_{fin}) \frac{1}{g_p g_Q} \sum_{k,l} |\mathcal{M}_{2,2}^{\text{on}}(p, q; i, j | p', q'; k, l)|^2(s, t) \\ &= \frac{p_{cm}}{2\sqrt{s}} \int d\Omega_{rel} \left(\frac{\|\mathbf{q} - \mathbf{q}'\|^2}{2} - \frac{p_{cm}^2}{2} (1 - \cos \theta)^2 \right) \frac{1}{g_p g_Q} \sum_{k,l} |\mathcal{M}_{2,2}^{\text{on}}(p, q; i, j | p', q'; k, l)|^2(s, t), \\ &= \frac{2\pi p_{cm}^3}{\sqrt{s}} \left(m_1(s) - m_2(s) \right), \end{aligned} \quad (\text{D.3})$$

and

$$\begin{aligned} b_{L,cm}(\mathbf{p}) &= \frac{p_{cm}}{\sqrt{s}} \int \frac{d^3 q'}{2E_{q'}} \int \frac{d^3 p'}{2E_{p'}} \left(\frac{((\mathbf{q} - \mathbf{q}') \cdot \hat{q})^2}{2} \right) \delta^{(4)}(P_{in} - P_{fin}) \frac{1}{g_p g_Q} \sum_{k,l} |\mathcal{M}_{2,2}^{\text{on}}(p, q; i, j | p', q'; k, l)|^2(s, t) \\ &= \frac{p_{cm}}{\sqrt{s}} \int d\Omega_{rel} \left(\frac{p_{cm}^2}{2} (1 - \cos \theta)^2 \right) \frac{1}{g_p g_Q} \sum_{k,l} |\mathcal{M}_{2,2}^{\text{on}}(p, q; i, j | p', q'; k, l)|^2(s, t), \\ &= \frac{4\pi p_{cm}^3}{\sqrt{s}} m_2(s), \end{aligned} \quad (\text{D.4})$$

where we have defined:

$$\begin{aligned} m_1^{\text{on}}(s) &= \int_{-1}^1 d\cos \theta \frac{1 - \cos \theta}{2} \sum |\mathcal{M}^{\text{on}}|^2 = \frac{1}{8p_{cm}^4} \int_{-4p_{cm}^2}^0 \sum |\mathcal{M}^{\text{on}}|^2(s, t) \times (-t) dt \\ m_2^{\text{on}}(s) &= \int_{-1}^1 d\cos \theta \left(\frac{1 - \cos \theta}{2} \right)^2 \sum |\mathcal{M}^{\text{on}}|^2 = \frac{1}{32p_{cm}^6} \int_{-4p_{cm}^2}^0 \sum |\mathcal{M}^{\text{on}}|^2(s, t) t^2 dt. \end{aligned} \quad (\text{D.5})$$

Using a Lorentz boost we transform b_{cm}^{ij} in eq.(D.2), with $b_{T,cm}(\mathbf{p})$ and $b_{L,cm}(\mathbf{p})$ given by (D.3) and (D.4), respectively, to the heavy-quark rest frame. Together with the remaining integral in $\mathcal{B}^{\mu\nu}$ (VI.1), one can prove that $\mathcal{B}^{\mu\nu}$ is expressed in the heavy-quark rest frame by

$$\mathcal{B}_{rest}^{\mu\nu} = \frac{M_Q^2}{16(2\pi)^4} \int \frac{q^5 dq}{s^2 E_q} \int d\Omega_{rel} f_r(\mathbf{q}) \left[\left(m_1(s) - m_2(s) \right) (I - |\hat{q}_{cm} \rangle \langle \hat{q}_{cm}|)^{\mu\nu} + 2m_2(s) \tilde{a}^\mu \tilde{a}^\nu \right] \quad (\text{D.6})$$

with \tilde{a}^μ is the a 4-vector defined by

$$\tilde{a}^\mu = \left(\frac{q}{\sqrt{s}}, \frac{M_Q + E_q}{\sqrt{s}} \hat{\mathbf{q}}_{cm} \right). \quad (\text{D.7})$$

Averaging over \hat{q}_{cm} , $\mathcal{B}_{rest}^{\mu\nu}$ can be written in the basis $|\hat{u} > \hat{u}|$, where u is the fluid velocity in the heavy quark rest frame as

$$\begin{aligned} \mathcal{B}_{rest}^{\mu\nu} = \frac{M_Q^2}{8(2\pi)^3} \int \frac{q^5 dq}{s^2 E_q} \left\{ 2 m_2(s) \begin{pmatrix} \frac{q^2}{s} f_0 & f_1 \frac{q(M_Q + E_q)}{s} \hat{u} \\ f_1 \frac{q(M_Q + E_q)}{s} \hat{u} & 0 \end{pmatrix} \right. \\ \left. + \left[\left(\frac{m_1(s) - m_2(s)}{2} \right) (f_0 + f_2) + \frac{(M_Q + E_q)^2}{s} m_2(s) (f_0 - f_2) \right] (I - |\hat{u} > \hat{u}|) \right. \\ \left. + \left[\left(m_1(s) - m_2(s) \right) (f_0 - f_2) + \frac{2(M_Q + E_q)^2}{s} m_2(s) f_2 \right] |\hat{u} > \hat{u}| \right\}, \end{aligned} \quad (\text{D.8})$$

with

$$f_i = \frac{1}{2} \int d\cos\theta f\left(\frac{u^0 E_q - uq\cos\theta}{T}\right) \cos^i\theta, \quad i \in [0, 1, 2]. \quad (\text{D.9})$$

Finally, a Lorentz boost of $\mathcal{B}_{rest}^{\mu\nu}$ eq.(D.8) with $(\gamma_u \beta_u = \mathbf{p}/M_Q, \gamma_u = E_p/M_Q)$ allows to determine $\mathcal{B}^{\mu\nu}$ in the heat bath rest frame. For the partial parts of $\mathcal{B}_{\text{heat bath}}^{\mu\nu}$, one finds

$$B_{T,\text{heat bath}}(\mathbf{p}) = \frac{M_Q^3}{8(2\pi)^3 E_Q} \int \frac{q^5 dq}{s^2 E_q} \left[\frac{m_1(s) - m_2(s)}{2} (f_0 + f_2) + \frac{(E_q + M_Q)^2}{s} m_2(s) (f_0 - f_2) \right] \quad (\text{D.10})$$

$$B_{L,\text{heat bath}}(\mathbf{p}) = \frac{M_Q^3}{8(2\pi)^3 E_Q} \int \frac{q^5 dq}{s^2 E_q} \left[\left(m_1(s) - m_2(s) \right) (f_0 - f_2) u_0^2 + \frac{2m_2(s)}{s} \left((E_q + M_Q)^2 u_0^2 f_2 - 2u_0 u q (E_q + M_Q) f_1 + u^2 q^2 f_0 \right) \right].$$

\hat{q}^{on} which is proportional to B_T (cf. eq.(VI.4)) is then given in the heat bath rest frame by [54]:

$$\hat{q}^{on}(p) = \frac{M_Q^3}{2(2\pi)^3 p_Q} \int_0^{+\infty} \frac{q^5}{s^2 E_q} \left[\frac{m_1^{on}(s) - m_2^{on}(s)}{2} (f_0 + f_2) + \frac{(E_q + M_Q)^2}{s} m_2^{on}(s) (f_0 - f_2) \right] dq. \quad (\text{D.11})$$

-
- [1] J. Adams *et al.* (STAR Collaboration), *Nucl.Phys.* **A757**, 102 (2005).
 - [2] K. Adcox *et al.* (PHENIX Collaboration), *Nucl.Phys.* **A757**, 184 (2005).
 - [3] B. Back, M. Baker, M. Ballintijn, D. Barton, B. Becker, *et al.*, *Nucl.Phys.* **A757**, 28 (2005).
 - [4] I. Arsene *et al.* (BRAHMS Collaboration), *Nucl.Phys.* **A757**, 1 (2005).
 - [5] W. Zajc, *Nucl.Phys.* **A805**, 283 (2008).
 - [6] W. Cassing and E. Bratkovskaya, *Phys.Rev.* **C78**, 034919 (2008).
 - [7] A. K. Dutt-Mazumder, J.-e. Alam, P. Roy, and B. Sinha, *Phys.Rev.* **D71**, 094016 (2005).
 - [8] M. G. Mustafa, *Phys.Rev.* **C72**, 014905 (2005).
 - [9] B. Svetitsky, *Phys.Rev.* **D37**, 2484 (1988).
 - [10] H. van Hees and R. Rapp, *Phys.Rev.* **C71**, 034907 (2005).
 - [11] G. D. Moore and D. Teaney, *Phys.Rev.* **C71**, 064904 (2005).
 - [12] H. van Hees, V. Greco, and R. Rapp, *Phys.Rev.* **C73**, 034913 (2006).
 - [13] P. B. Gossiaux, V. Guiho, and J. Aichelin, *J.Phys.* **G31**, S1079 (2005).
 - [14] P. Gossiaux, V. Guiho, and J. Aichelin, *J.Phys.* **G32**, S359 (2006).
 - [15] N. Armesto, M. Cacciari, A. Dainese, C. A. Salgado, and U. A. Wiedemann, *Phys.Lett.* **B637**, 362 (2006).
 - [16] H. van Hees, M. Mannarelli, V. Greco, and R. Rapp, *Phys.Rev.Lett.* **100**, 192301 (2008).
 - [17] D. Molnar, *J.Phys.* **G31**, S421 (2005).
 - [18] B.-W. Zhang, E. Wang, and X.-N. Wang, *Phys.Rev.Lett.* **93**, 072301 (2004).
 - [19] P. Gossiaux and J. Aichelin, *Phys.Rev.* **C78**, 014904 (2008).
 - [20] P. Gossiaux and J. Aichelin, *J.Phys.* **G36**, 064028 (2009).
 - [21] O. Linnyk, E. Bratkovskaya, and W. Cassing, *Int.J.Mod.Phys.* **E17**, 1367 (2008).

- [22] S. Wicks, W. Horowitz, M. Djordjevic, and M. Gyulassy, *Nucl.Phys.* **A784**, 426 (2007).
- [23] P. B. Gossiaux and J. Aichelin, *Phys. Rev. C* **78**, 014904 (2008).
- [24] J. Bielcik (STAR Collaboration), *Nucl.Phys.* **A774**, 697 (2006).
- [25] S. Adler *et al.* (PHENIX Collaboration), *Phys.Rev.Lett.* **96**, 032301 (2006).
- [26] R. Rapp and H. van Hees, Mar 2009. 95 pp. Published in R. C. Hwa, X.-N. Wang (Ed.) *Quark Gluon Plasma 4*, World Scientific, 111 (2010) e-Print:, [arXiv:0903.1096](https://arxiv.org/abs/0903.1096) [hep-ph].
- [27] P. B. Gossiaux, S. Vogel, H. van Hees, J. Aichelin, R. Rapp, *et al.*, (2011), [arXiv:1102.1114](https://arxiv.org/abs/1102.1114) [hep-ph].
- [28] H. Berrehrah, E. Bratkovskaya, W. Cassing, P. Gossiaux, J. Aichelin, *et al.*, *Phys.Rev.* **C89**, 054901 (2014).
- [29] P. Gossiaux, R. Bierkandt, and J. Aichelin, *Phys.Rev.* **C79**, 044906 (2009).
- [30] Y. L. Dokshitzer, G. Marchesini, and B. Webber, *Nucl.Phys.* **B469**, 93 (1996).
- [31] E. Braaten and M. H. Thoma, *Phys. Rev. D* **44**, R2625 (1991).
- [32] B. Combridge, *Nuclear Physics B* **151**, 429 (1979).
- [33] S. Peigne and A. Peshier, *Phys.Rev.* **D77**, 114017 (2008).
- [34] A. Peshier, *Phys. Rev. D* **70**, 034016 (2004).
- [35] A. Peshier, *Journal of Physics G: Nuclear and Particle Physics* **31**, S371 (2005).
- [36] W. Cassing, O. Linnyk, T. Steinert, and V. Ozvenchuk, *Phys. Rev. Lett.* **110**, 182301 (2013).
- [37] W. Cassing, *The European Physical Journal Special Topics* **168**, 3 (2009).
- [38] W. Cassing and E. Bratkovskaya, *Nucl.Phys.* **A831**, 215 (2009).
- [39] W. Cassing, *Nuclear Physics A* **791**, 365 (2007).
- [40] W. Cassing and E. Bratkovskaya, *Nuclear Physics A* **831**, 215 (2009).
- [41] S. Borsanyi *et al.* (Wuppertal-Budapest Collaboration), *JHEP* **1009**, 073 (2010).
- [42] S. Borsanyi, G. Endrodi, Z. Fodor, A. Jakovac, S. D. Katz, *et al.*, *JHEP* **1011**, 077 (2010).
- [43] V. Ozvenchuk, O. Linnyk, M. I. Gorenstein, E. L. Bratkovskaya, and W. Cassing, *Phys. Rev. C* **87**, 024901 (2013).
- [44] M. Golam Mustafa, D. Pal, and D. Kumar Srivastava, *Phys.Rev.* **C57**, 889 (1998).
- [45] D. B. Walton and J. Rafelski, *Phys.Rev.Lett.* **84**, 31 (2000).
- [46] V. Greco, H. van Hees, and R. Rapp, (2007), [arXiv:0709.4452](https://arxiv.org/abs/0709.4452) [hep-ph].
- [47] W. Horowitz and M. Gyulassy, *J.Phys.* **G35**, 104152 (2008).
- [48] S. S. Gubser, *Phys.Rev.* **D76**, 126003 (2007).
- [49] H. Ding, A. Francis, O. Kaczmarek, F. Karsch, H. Satz, *et al.*, *Phys.Rev.* **D86**, 014509 (2012).
- [50] A. Beraudo, A. De Pace, W. Alberico, and A. Molinari, *Nucl.Phys.* **A831**, 59 (2009).
- [51] J. Casalderrey-Solana and D. Teaney, *JHEP* **0704**, 039 (2007).
- [52] S. S. Gubser, *Nucl.Phys.* **B790**, 175 (2008).
- [53] H. Liu, K. Rajagopal, and Y. Shi, *JHEP* **0808**, 048 (2008).
- [54] P.B. Gossiaux, *Pertes d'énergie et effet de retard*, Habilitation report (*Tomographie du Plasma de Quarks et de Gluons Grâce aux Saveurs Lourdes : Éléments de Théorie, Phénoménologie et Applications*), 2009.
- [55] K. Sergey, (2014), [arXiv:1404.5476](https://arxiv.org/abs/1404.5476) [physics.chem-ph].
- [56] F. Reif, *Fundamentals of Statistical and Thermal Physics* (McGraw-Hill, New York, 1965).
- [57] R. Marty, E. Bratkovskaya, W. Cassing, J. Aichelin, and H. Berrehrah, *Phys.Rev.* **C88**, 045204 (2013).